

RESEARCH ARTICLE

10.1002/2015MS000446

Key Points:

- Deep tropical convection is sensitive to the thermodynamic environment
- Atmospheric stability determines the convective profile in WTG simulations
- Parameterization scheme for horizontal moisture advection modifies convection

Correspondence to:

S. L. Sessions,
sessions@kestrel.nmt.edu

Citation:

Sessions, S.L., M. J. Herman, and S. Sentić (2015), Convective response to changes in the thermodynamic environment in idealized weak temperature gradient simulations, *J. Adv. Model. Earth Syst.*, 7, 712–738, doi:10.1002/2015MS000446.

Received 26 FEB 2015

Accepted 17 APR 2015

Accepted article online 24 APR 2015

Published online 19 MAY 2015

Convective response to changes in the thermodynamic environment in idealized weak temperature gradient simulations

Sharon L. Sessions¹, Michael J. Herman¹, and Stipo Sentić¹

¹Department of Physics and Geophysical Research Center, New Mexico Tech, Socorro, New Mexico, USA

Abstract We investigate the response of convection to idealized perturbations in the thermodynamic environment in simulations which parameterize the large-scale circulations using the weak temperature gradient (WTG) approximation. The perturbations include a combination of modifying the environmental moisture and atmospheric stability via imposing anomalies in reference moisture and temperature profiles. We find that changes in atmospheric stability strongly influence the character of convection by drastically modifying the vertical motion profile, whereas changes to atmospheric moisture modulate the intensity of precipitation produced by the convection, but do not qualitatively change the shape of the vertical motion profile. An important question is how does horizontal moisture advection into the domain affect convection? We test several different parameterizations of this process; these include lateral entrainment by circulations induced by enforcing WTG, a moisture relaxation which parameterizes the advection of moisture by large-scale nondivergent circulations, and control simulations in which both of these mechanisms are turned off so horizontal advection is assumed negligible compared to vertical advection. Interestingly, the most significant differences resulting from the choice of horizontal moisture advection scheme appear in environmental conditions which suppress—rather than support—the development of deep tropical convection. In this case, lateral entrainment related to WTG circulations is the only parameterization which results in extreme drying of the troposphere in environments which suppress convection. Consequently, this is the only parameterization which permits multiple equilibria—dry or precipitating steady states—in convection.

1. Introduction

Understanding the interaction between deep tropical convection and the large-scale environment benefits our knowledge of the tropical atmosphere and leads to improvements in the convective parameterizations in numerical models used for weather forecasting and climate prediction. This interaction is two-way: convection fuels waves that drive the large-scale transport, while the large-scale circulation sets the environment for convection. In this work, we focus on the latter part of this interaction and investigate how the characteristics of convection respond to changes in the large-scale thermodynamic environment, where the large-scale environment is parameterized using the weak temperature gradient approximation [Sobel and Bretherton, 2000; Raymond and Zeng, 2005].

The weak temperature gradient (WTG) approximation is based on the observation that horizontal temperature gradients are small in the tropical atmosphere where gravity waves act to balance convective heating and radiative cooling. Models employing the WTG approximation achieve this balance by generating a domain-mean vertical velocity that counteracts buoyancy anomalies produced by diabatic processes. This WTG vertical velocity—and thus the modeled convection—is sensitive to changes in the reference profiles of potential temperature and moisture which represent the thermodynamic environment [Mapes, 2004; Raymond and Sessions, 2007; Wang and Sobel, 2012; Emanuel et al., 2013; Wang et al., 2013; Herman and Raymond, 2014]. It is also sensitive to the model and the specific implementation of WTG [Daleu et al., 2012; Herman and Raymond, 2014], as well as to details of how horizontal moisture advection is parameterized [Sobel and Bretherton, 2000; Sobel et al., 2007].

The purpose of this investigation is twofold: (1) to diagnose the changes in convection modeled in different thermodynamic environments using the WTG approximation, and (2) to determine how different choices

© 2015. The Authors.

This is an open access article under the terms of the Creative Commons Attribution-NonCommercial-NoDerivs License, which permits use and distribution in any medium, provided the original work is properly cited, the use is non-commercial and no modifications or adaptations are made.

for parameterizing horizontal moisture advection affect the convection. We also consider how these influence the existence of multiple equilibria in precipitation.

Several modeling studies have demonstrated the sensitivity of convection to the thermodynamic environment—characterized here by atmospheric stability and humidity. *Mapes* [2004] used a cloud-resolving model to investigate the transient rainfall response to deep vertical and vertical-dipole perturbations in potential temperature and water vapor mixing ratio. While both of these perturbations—representing first and second baroclinic mode vertical displacements, respectively—generated transient responses in rainfall, *Mapes* [2004] found that the vertical-dipole perturbations enhanced the transient rainfall response compared to deep vertical displacements. *Raymond and Sessions* [2007] and *Herman and Raymond* [2014] showed that more stable environments produce more bottom-heavy convection with increased precipitation rates, while more moist environments produce more intense convection without changing the altitude of the maximum mass flux. An interesting contrast is found in results of *Wang and Sobel* [2012], who showed that strong lower tropospheric drying can reduce top-heaviness and ultimately prevent deep convection entirely, though this did not occur in a similar investigation when convection was also parameterized [*Sobel and Bellon*, 2009].

The sensitivity of convection to the thermodynamic environment is not unique to WTG simulations; alternate parameterizations of the large-scale also produce responses broadly consistent with WTG simulations. For example, *Kuang* [2010] computed linear response functions based on the response of convection to temperature and moisture perturbations. His results were corroborated in a parallel study by *Tulich and Mapes* [2010], who considered transient sensitivities of convection to sudden perturbations in temperature and moisture.

Idealized studies which investigate how convection responds to prescribed changes in the thermodynamic environment—and how the response depends on the implementation of WTG—provide valuable insight for identifying mechanisms involved in convective processes. These studies also provide a framework for interpreting WTG simulations which incorporate observed anomalies in reference profiles of WTG simulations, such as those used to study the Madden-Julian Oscillation [*Wang et al.*, 2013].

Previous studies have demonstrated the importance of vertical moisture advection on the existence of convectively coupled waves [e.g., *Kuang*, 2008]. Another important aspect of this work is to determine how the sensitivities of convection to the thermodynamic environment depend on the method used to parameterize horizontal moisture advection. This is potentially important for improving the representation of convection in global models [*Derbyshire et al.*, 2004], as well as for improving the simulation of the Madden-Julian Oscillation [*Pritchard and Bretherton*, 2014; *Zhu and Hendon*, 2015].

Another important application of WTG simulations is investigating whether a particular set of parameters support multiple equilibria in precipitation. Multiple equilibria refers to the ability of a model to either sustain a dry or precipitating steady state under identical boundary conditions; the state realized by the model depends on the initial moisture profile in the model [*Sobel et al.*, 2007; *Sessions et al.*, 2010; *Emanuel et al.*, 2013; *Herman and Raymond*, 2014]. Previous studies indicate that the existence of multiple equilibria depends on the degree to which WTG is enforced [*Sessions et al.*, 2010], domain size [*Sessions et al.*, 2010], boundary layer depth [*Herman and Raymond*, 2014], how environmental moisture is chosen to enter the domain [*Sobel et al.*, 2007], and the background sea surface temperature in which the multiple equilibria experiments are performed [*Emanuel et al.*, 2013], among other things.

Whether or not the thermodynamic environment or choice for horizontal moisture advection scheme affects the existence of multiple equilibria is important for understanding the relevance of these choices in large-scale representations. For example, multiple equilibria in WTG domains are believed to be analogous to convecting and dry regions of large domain radiative convective equilibrium simulations with self-aggregated convection [*Bretherton et al.*, 2005; *Muller and Held*, 2012; *Wing and Emanuel*, 2013; *Emanuel et al.*, 2013; *Jeevanjee and Romps*, 2013]. *Wing and Emanuel* [2013] and *Emanuel et al.* [2013] demonstrated the importance of the feedback between radiative cooling and water vapor in self-aggregation and multiple equilibria experiments, respectively; thus, identifying parameters which influence water vapor content in these WTG experiments may help identify mechanisms relevant for organizing convection.

This paper is organized as follows: We briefly introduce the weak temperature gradient approximation and its implementation in our model in section 2. In section 3, we describe the model and the series of

numerical experiments used for this work. Diagnostic quantities are defined in section 4, we present results in section 5, and we summarize and discuss the consequences of our results in section 6.

2. Weak Temperature-Gradient (WTG) Approximation

The weak temperature-gradient (WTG) approximation is a useful tool for investigating convection in limited domain simulations [Sobel and Bretherton, 2000; Raymond and Zeng, 2005]. This work uses an implementation of WTG similar to that used by Raymond and Zeng [2005], but with some significant upgrades which primarily result in changes to the source terms in the equations governing the equivalent potential temperature, θ_e , and the total water mixing ratio, r_t . For the purpose of this work, the most important changes are: different representations for parameterizing horizontal moisture advection from the environment into the model domain (“moisture treatment”); and performance improvements and bug fixes (described in the model documentation, not here). These changes are documented in Herman and Raymond [2014]; though we summarize those pertinent to this work here.

The thermodynamic equations for equivalent potential temperature, θ_e , and total water mixing ratio, r_t , are:

$$\frac{\partial \rho \theta_e}{\partial t} + \nabla \cdot (\rho \mathbf{v} \theta_e - K \nabla \theta_e) = \rho (S_{es} + S_{er} - S_e) \quad (1)$$

and

$$\frac{\partial \rho r_t}{\partial t} + \nabla \cdot (\rho \mathbf{v} r_t - K \nabla r_t) = \rho S_{cr} + \rho (S_{rs} - S_r). \quad (2)$$

Here, ρ is the density, \mathbf{v} is the velocity, and K is the eddy mixing coefficient. S_{es} is the source of equivalent potential temperature from surface fluxes; S_{er} is the source of θ_e from radiation. S_{rs} is the source of total cloud water from surface evaporation; S_{cr} is minus the conversion rate of cloud water to precipitation. S_e and S_r are sinks of equivalent potential temperature and total water mixing ratio due to external sources; these are a consequence of enforcing the WTG approximation. The domain mean potential temperature, $\bar{\theta}$, is relaxed to a reference profile representing the large-scale, θ_0 . This relaxation is initiated by a potential temperature anomaly, $(\bar{\theta} - \theta_0)$, that accounts for radiative cooling and convective heating within the model domain. This modulates a potential temperature sink, S_θ :

$$S_\theta = \lambda_\theta M(z) (\bar{\theta} - \theta_0). \quad (3)$$

Here $1/\lambda_\theta$ is the time scale over which the domain mean potential temperature relaxes to the reference profile; physically it represents the time over which gravity waves would redistribute buoyancy anomalies. $M(z) = \sin(\pi z/H)$ is a masking function which modulates the relaxation. It is applied only to the vertical layer $b < z < H$, where b is the height of the boundary layer top and H is the tropopause height. Above H , M is set to zero. The temperature anomaly diagnosed in equation (3) then generates a vertical velocity that counteracts the heating via adiabatic cooling. This velocity is the weak temperature gradient vertical velocity, w_{wtg} , defined as:

$$w_{wtg} = \left(\frac{\partial \bar{\theta}}{\partial z} \right)^{-1} S_\theta. \quad (4)$$

Strictly speaking, the WTG approximation is based on weak horizontal gradients in virtual temperature, not potential temperature. The model used in this study does not include the effects of water vapor on buoyancy. However, some simple tests (for example, defining w_{wtg} in terms of virtual potential temperature instead of potential temperature) indicate that this is a small error (well within model variability), and thus excluding buoyancy effects of moisture are unlikely to qualitatively affect the results of this work.

The parameterized vertical velocity in equation (4) vertically advects θ_e and moisture. Since the WTG vertical velocity is assumed to satisfy the anelastic mass continuity equation, vertical motion can induce horizontal convergence of environmental air into the model domain. This contributes to external sources, S_e and S_r , in equations (1) and (2). The specific form of these is given in section 3.3, where we discuss options for moisture treatment. In the boundary layer, convective heating is shallow and the corresponding gravity waves are slow [Bretherton and Smolarkiewicz, 1989]. Consequently, WTG is not a good approximation for the

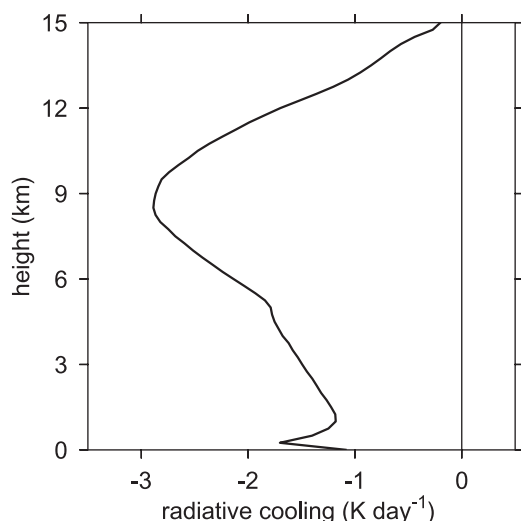


Figure 1. Mean radiative cooling profile from a radiative convective equilibrium (RCE) simulation. This cooling profile is the prescribed static cooling for all experiments in this work.

boundary layer, so for $z < b$ the WTG vertical velocity is linearly interpolated in height from its value at b to zero at the surface.

3. Numerical Experiments

In this section, we describe the implementation of WTG in our model and the experiments used in this investigation.

3.1. Model Set Up

All numerical experiments in this study are conducted using two-dimensional geometry. The horizontal dimension is 200 km with 1 km grid resolution; the vertical spans 20 km with 250 m resolution. We choose to use two-dimensional domains for computational efficiency; previous studies have shown that they give qualitatively similar results as their three-dimensional counterparts [Wang and Sobel, 2011], and are therefore sufficient for this study.

All simulations use a uniform SST of 303 K. The model is run in non-WTG mode until the convective heating balances radiative cooling (radiative convective equilibrium, RCE). The RCE profiles are calculated with interactive radiation using the toy radiation scheme of Raymond and Torres [1998], and a mean surface wind speed of 5 m s^{-1} . The strength of convection is modulated through surface fluxes which can be increased by increasing sea surface temperatures (SSTs) or surface wind speeds. To investigate the characteristics of convection in WTG mode, it is useful to increase the surface fluxes relative to the value used in the RCE calculation so the model exhibits stronger convective heating compared to radiative cooling. We choose to increase the surface wind speed to 7 m s^{-1} for most simulations, up to 10 m s^{-1} for multiple equilibria experiments (see below).

Although the RCE simulations invoke interactive radiation, we choose to perform all WTG simulations with noninteractive (static) radiative cooling. The radiative cooling profile is taken as the time and domain mean of the RCE simulation, see Figure 1. Static radiative cooling in the WTG simulations allows us to isolate the effect of changes in the thermodynamic environment and moisture treatment independent of the changes to the cooling profile that would occur with radiative feedbacks. Using the RCE cooling profile—rather than a cooling profile that is held constant with height in the troposphere—allows the convection to respond to a cooling profile that is more representative of the model environment.

Finally, we must specify the time scale over which the domain-averaged potential temperature is relaxed to the reference profile ($1/\lambda_\theta$ in equation (3)). $\lambda_\theta \rightarrow \infty$ represents a strict enforcement of WTG ($\bar{\theta} = \theta_0$), while $\lambda_\theta \rightarrow 0$ turns WTG off and allows the model to approach RCE. We choose a relaxation time scale of approximately 11 min ($\lambda_\theta = 1.5 \times 10^{-3} \text{ s}^{-1}$). This is a much shorter time scale than is typical of WTG experiments, which range from 1–3 h [Sessions et al., 2010; Wang and Sobel, 2011, 2012; Daleu et al., 2012; Anber et al., 2014; Herman and Raymond, 2014], though Sobel et al. [2007] used strict enforcement of WTG (0 h). Sessions et al. [2010] considered a range of time scales (0.01–3.5 h) and found that shorter time scales permit a larger range of multiple equilibria; part of the reason we choose a time scale that is much shorter than typical values is because we are considering multiple equilibria in this work. Furthermore, a stricter enforcement of WTG forces convection to be more sensitive to the thermodynamic environment, and is thus conducive for investigating the response of convection to changes in the environment. We expect that a longer relaxation time would decrease the magnitude of the response, but would not qualitatively change the results. This is supported by the WTG simulations of Romps [2012b], who found that different time scales (5 and 30 min) affected the magnitude—but not the overall shape—of the WTG vertical velocity profile.

As we mentioned previously, the WTG relaxation time scale represents the time it takes gravity waves to neutralize buoyancy anomalies. This corresponds to a distance for a given gravity wave speed; however, it is

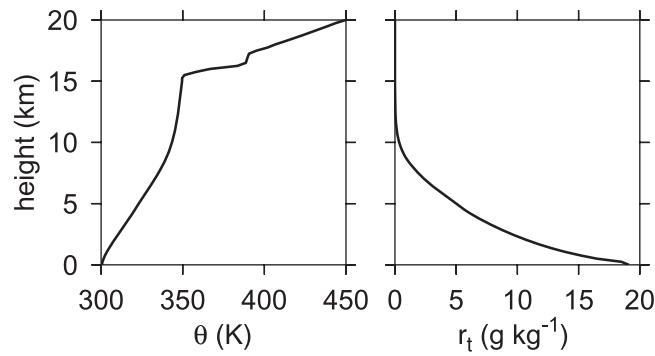


Figure 2. Radiative convective equilibrium (RCE) profiles of potential temperature (left) and total water mixing ratio (right) used as unperturbed reference profiles in WTG calculations. RCE is calculated over a uniform SST of 303 K, with surface wind speed of 5 m s⁻¹ and interactive radiation on a 2-D, 200 km horizontal domain.

potential temperature and total water mixing ratio representative of the convective environment (θ_0 and r_{t0} in equations (3) and (6)). The reference profiles are generated by running the model to RCE in non-WTG mode (i.e., $\lambda_\theta=0$ in equation (3); and $\lambda_{hadv}=\lambda_m=0$ in equation (6)). Time and domain averages of potential temperature and total water mixing ratio give the reference profiles $\theta_0(z)$ and $r_0(z)$, shown in Figure 2 for RCE simulations. The time average is taken over the last 30 days of a 1 year simulation.

In order to investigate the response of convection to changes in the reference environment, we perform numerical experiments similar to *Raymond and Sessions* [2007]. *Raymond and Sessions* [2007] showed that either moistening or stabilizing the environment resulted in increased precipitation rates for given surface fluxes; increasing the reference moisture increased the magnitude of the vertical mass flux without changing the shape, while increasing the stability both increased the magnitude of the vertical mass flux and lowered the level of maximum mass flux, resulting in more “bottom-heavy” convection. As a consequence, this concentrates the convergence to low levels where the air is more moist, resulting in a higher precipitation efficiency.

Raymond and Sessions [2007] represented changes to the reference environment by adding idealized perturbations to either the potential temperature or the mixing ratio reference profiles. An increase in the atmospheric stability was produced by specifying a cooling of $\delta\theta=2$ K centered at $h=3$ km and a warming of the same magnitude centered at $h=10$ km. The form of the perturbation centered at level h is given by:

$$\Delta\theta=\delta\theta\left(\frac{z}{h}\right)^2 e^{[2(1-z/h)]}, \tag{5}$$

where z is the altitude. In addition to a more stable environment, we also explore the impact of a less stable environment with perturbations of the same magnitude but with opposite signs (warming of 2 K at 3 km with cooling of 2 K at 10 km).

Moistening or drying is achieved by modifying the reference mixing ratio profile with a perturbation similar to equation (5), but with $\delta\theta$ replaced by δr , where $\delta r=\pm 1.0$ g kg⁻¹ and $h=3$ km. This choice is consistent with the moisture perturbations of *Raymond and Sessions* [2007], and is similar to the lower tropospheric drying level used in *Wang and Sobel* [2012]. In order to explore the full range of possible environments, we perform sets of nine experiments which account for all combinations of perturbations to the reference potential temperature and moisture profiles. These combinations are shown in Figure 3. The symbols in the top right corners of each plot represent the modifications to the reference profiles. Environmental stability is represented by the geometric stability of the symbols:

1. the completely unperturbed RCE profiles (Figure 3, control, middle plot) are represented by a bulls-eye;
2. more stable environments (Figure 3, top row) are represented by upright triangles (geometrically more stable shapes);
3. less stable environments (Figure 3, bottom row) are represented by inverted triangles (geometrically unstable shapes);

not clear what the appropriate distance is. The scale of the convective disturbance [*Romps*, 2012a, 2012b] and the spacing between disturbances [*Bretherton and Smolarkiewicz*, 1989; *Cohen and Craig*, 2004] are possible candidates. Gravity waves traveling at 50 m s⁻¹ travel 33 km in 11 min. Depending on what the appropriate length scale is, the time scale used in this study may be physically reasonable.

3.2. Reference Profiles

In the WTG approximation, we must specify reference profiles of

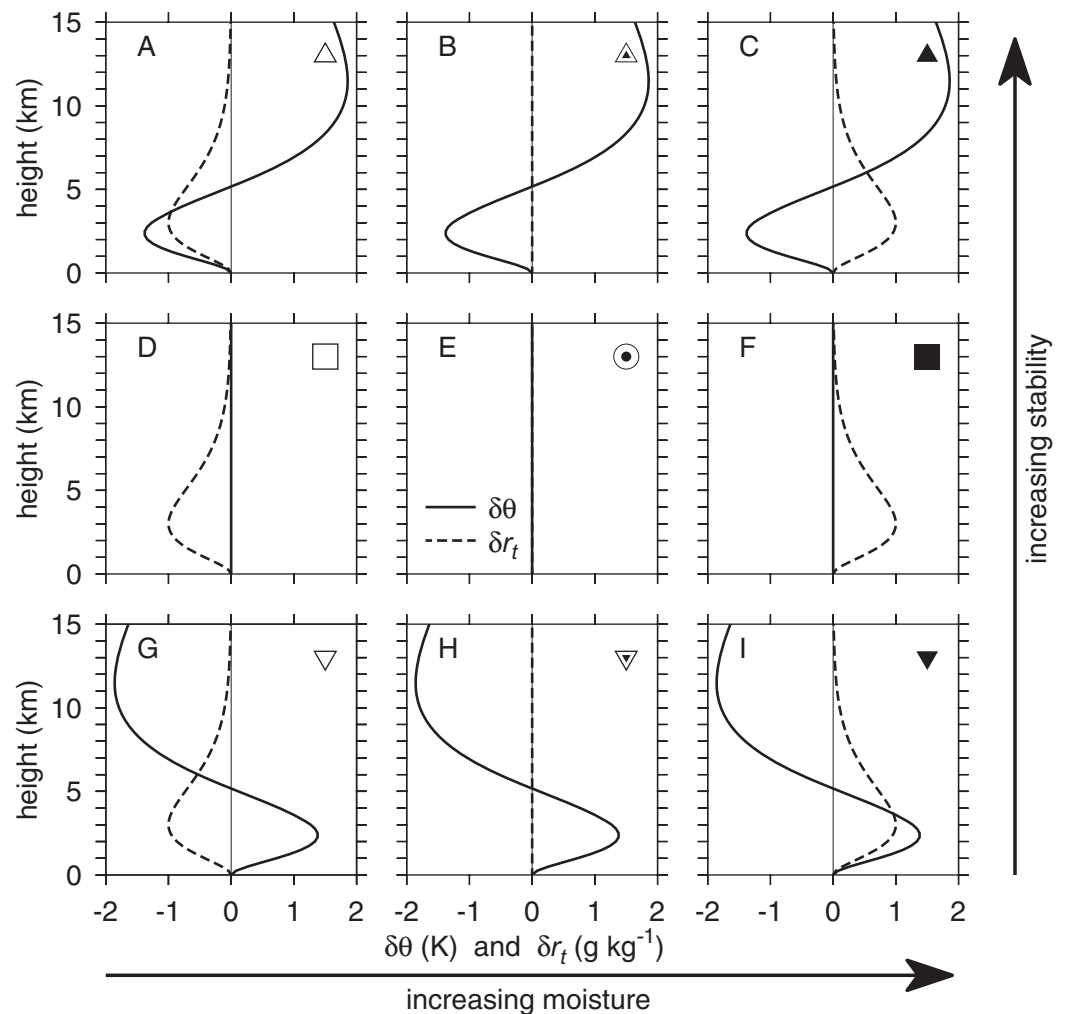


Figure 3. Perturbations added to the RCE reference profile. Solid lines represent perturbations to the potential temperature profiles, dashed lines give mixing ratio perturbations. The middle plot is the unperturbed RCE reference state. The middle row has unperturbed reference potential temperature profiles, the top row has perturbations representing more stable environments, and the bottom row represents less stable environments. Similarly, the middle column has no perturbations added to the reference moisture environment, the left column is drier, and the right column, moister. The symbols in the top right of each plot represent the reference environment. The shading represents the moisture perturbation: empty symbols are drier, full symbols are moister, half-filled symbols have unperturbed moisture profiles. The squares are unperturbed θ profiles; more stable environments are represented by upright triangles (geometrically more stable shapes); less stable environments are represented by inverted triangles. In order to easily distinguish the unperturbed RCE profiles, we choose bulls-eyes to represent these simulations. This figure serves as a symbol legend for results presented in section 5.

4. an atmosphere with the stability of the RCE profile (Figure 3, middle row) is represented by squares (neutrally stable shapes).

The symbol shading indicates a moistening or drying of the reference environment. In analogy with a glass of water,

1. empty is drier;
2. half-filled is unperturbed; and
3. filled is moister.

These symbols serve as a legend for results presented in section 5.

Rather than doing individual experiments for each combination shown in Figure 3, experiments are run for 90 days with perturbations imposed in 30 day increments. For each combination of perturbations, two sets of 90 day experiments are run; the first month is unperturbed; the second month has *either* potential

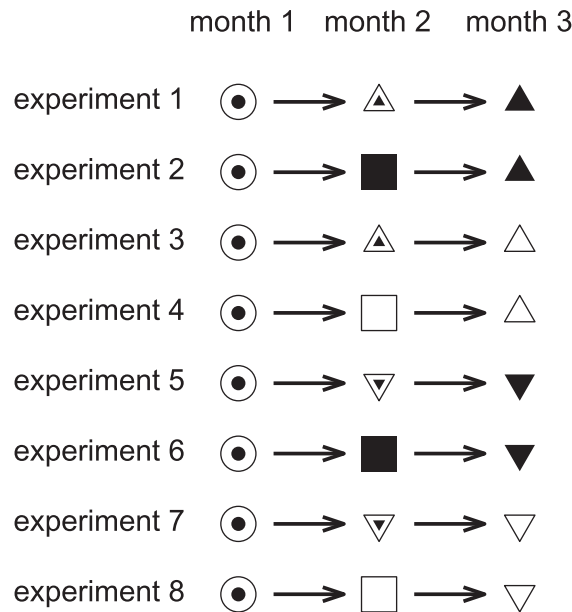


Figure 4. Graphic showing the sequence of perturbations applied in each experiment. Symbols are the same as in Figure 3: bulls-eyes are unperturbed profiles; squares indicate no change in stability; triangles indicate change in stability (upright are more stable); amount of filling represents environmental moisture perturbation with empty being drier and filled being moister.

temperature or moisture perturbed; the third month has *both* profiles perturbed. A set of eight experiments—graphically depicted in Figure 4—is required to represent all combinations of reference environments shown in Figure 3.

The time dependence in the experimental design has several advantages compared to individual experiments for each combination of perturbations:

1. It provides a minimum of two simulations with identical boundary conditions to confirm the uniqueness of the state for the given conditions (each combination of perturbations represented in Figure 3 is repeated at least twice; the unperturbed reference state is repeated 8 times).
2. It confirms that the state in month 3 is unique as it is reached from two distinct steady states in the previous month;
3. It gives a sense of variability when conditions are the same;
4. It gives temporal information for studying the transition itself as the conditions change (though this is not explicitly studied in this paper).

We choose 30 day increments to give enough time for the system to reequilibrate after the perturbation occurs, and enough simulation time to generate mean-state statistics. Statistics are taken from domain mean time averages over the last 2 weeks of each 30 day run (minus 1 h to avoid the ambiguous data at the transition). See section 5.1 for sample data showing precipitation rate as a function of time for the eight experiments depicted in Figure 4.

3.3. Moisture Treatment

The prognostic equation for total water mixing ratio (equation (2)) includes an external sink, S_r , which is a consequence of enforcing WTG. This external sink is given by

$$S_r = w_{wtg} \frac{\partial \bar{r}_t}{\partial z} + \lambda_{adv} (\bar{r}_t - r_x) \frac{1}{\rho_0} \frac{\partial \rho_0 w_{wtg}}{\partial z} + \lambda_m (\bar{r}_t - r_{t0}), \quad (6)$$

where

$$r_x = \begin{cases} \bar{r}_t & \text{if } \partial \rho_0 w_{wtg} / \partial z < 0 \quad (\text{detraining levels}) \\ r_{t0} & \text{if } \partial \rho_0 w_{wtg} / \partial z > 0 \quad (\text{entraining levels}) \end{cases} \quad (7)$$

The three terms on the right-hand side of equation (6) represent sinks of moisture due to large-scale vertical advection by the mean vertical velocity w_{wtg} , explicit lateral entrainment from the surrounding environment, and an imposed relaxation to the reference profile, r_{t0} which is independent of the WTG velocity.

As long as the model is operating in WTG mode and w_{wtg} is nonzero, moisture will be vertically advected within the domain (first term, equation (6)). Horizontal advection of moisture occurs either by lateral entrainment due to divergent circulations generated by enforcing mass continuity in the WTG velocity field (second term, equation (6)), or from large-scale flow that deposits dry or moist air into the domain independent of WTG circulations. The latter is parameterized by relaxing the domain mean moisture profile to the reference profile, r_{t0} (third term, equation (6)). Note that this relaxation occurs through the entire

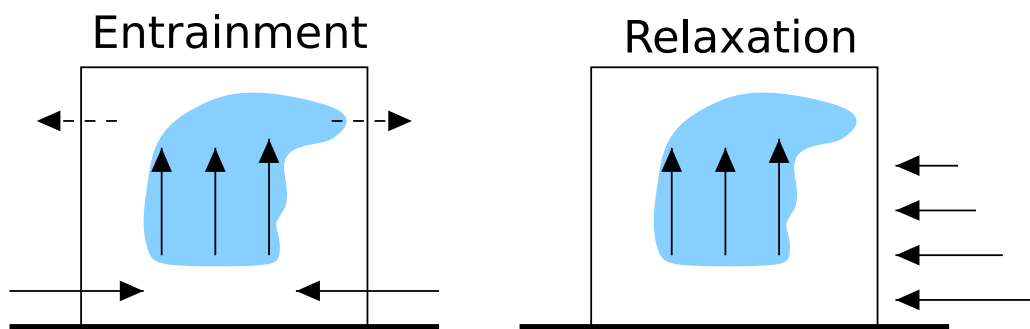


Figure 5. Cartoon representations of the physical processes captured by the different parameterizations of horizontal moisture advection. In each case, the box represents the domain of the CRM. Arrows pointing up represent the WTG vertical mass flux (ρW_{WTG}). The outside of each box represents the environment and therefore the reference profiles used in the WTG experiments. The left plot shows the lateral entrainment of the reference moisture at low levels which results from convergence via mass continuity in the WTG velocity field. The dashed arrows indicate the detrainment that would occur in the real atmosphere due to divergence in a layer where buoyancy decreases with height. Since detrainment of intrinsic quantities does not alter the modeled environment, there is no change in the moisture due to this mechanism (see equation (7)). The right plot illustrates how moisture might enter the domain from large-scale circulations that are independent of those induced by WTG; this process is parameterized by directly relaxing the domain mean moisture profile to the reference profile.

depth of the troposphere, not just at entraining levels. Figure 5 illustrates the difference between these processes.

The choice of horizontal moisture advection scheme is set by the values of λ_{hadv} and λ_m , which are specified externally. λ_{hadv} has values of either 0 or 1, to turn lateral entrainment off or on. Setting this to zero assumes the change in domain moisture via horizontal advection is small compared to that due to the vertical advection; a value of 1 laterally entrains moisture from the reference environment according to mass continuity of the WTG velocity field. $\lambda_m=0$ assumes horizontal moisture advection is purely divergent; a nonzero value relaxes the domain moisture to the reference profile over a timescale $1/\lambda_m$. Both of these choices have been employed in WTG experiments. *Raymond and Zeng* [2005]; *Raymond and Sessions* [2007]; *Sessions et al.* [2010]; *Wang et al.* [2013]; and *Herman and Raymond* [2014] have all implemented explicit lateral entrainment of environmental moisture. Other investigations which explicitly aimed to determine the effect of moisture (including drying) on convection have relaxed moisture to a specified profile [*Sobel et al.*, 2007; *Sobel and Bellon*, 2009; *Wang and Sobel*, 2012]. It is worth noting that *Sobel and Bretherton* [2000] investigated the effect of horizontal moisture advection by horizontal winds that were independent of WTG circulations; moisture relaxation parameterizes this mechanism.

Since the divergent and rotational flow are decoupled, both effects may influence convection and we either choose one mechanism to represent the horizontal moisture advection, or we can simultaneously allow both to be turned on ($\lambda_{hadv}=1$, $\lambda_m \neq 0$) since both of these mechanisms may be at work in the real environment. In principle, the source due to large-scale motions associated with the direct relaxation may have a unique reference profile that represents the moisture in an environment upstream from the convecting domain. Since we do not have a reference profile to represent the upstream moisture, we simply assume that the reference profile represents the moisture immediately available to the convective domain, and we use this for both lateral entrainment and moisture relaxation. Using this configuration, lateral entrainment and moisture relaxation will usually act in concert to either increase or decrease domain moisture, but in some conditions, these mechanisms may compete and result in opposite tendencies (see section 5). In either case, when the WTG vertical velocity is zero or else implies divergence via equation (7), the entrainment is shut off.

Alternatively, if we assume the horizontal contributions are small compared to the vertical advection of moisture, we can shut off both moisture schemes ($\lambda_{hadv}=0$, $\lambda_m=0$). This is equivalent to an implicit horizontal moisture advection where moisture is advected into the domain via circulations that obey mass continuity, but they advect moisture from an environment that has a moisture profile identical to that in the model domain. The moisture profile of the domain is a result of a combination of surface evaporation, vertical advection by the WTG vertical velocity, and evaporation of precipitation, so in this case, the environmental moisture is determined by the modeled convection, and it is independent of an externally specified reference moisture profile. This has been a popular choice in previous studies [e.g., *Sobel and Bretherton*, 2000; *Sobel et al.*, 2007;

Wang and Sobel, 2011; Wang et al., 2013; Anber et al., 2014]. Because this is the only moisture treatment which does not depend on a reference moisture profile, we refer to this as the control method.

For the simulations which include moisture relaxation, we choose a relaxation time scale of 1.8 days. To establish the moisture relaxation time scale, we conducted experiments over a range of moisture relaxation time scales and compared the modeled precipitation rate to the values produced using lateral moisture entrainment. Unperturbed environments were not sensitive to the relaxation time chosen, but smaller relaxation times gave higher precipitation rates for more moist or more stable environments. $1/\lambda_m = 1.8$ days represents the relaxation time that gives precipitation rates closest to those produced using lateral entrainment. It is important to note that strictly enforcing the moisture profile ($1/\lambda_m = 0$) shuts off the precipitation entirely because the reference profile is unsaturated and thus cannot trigger precipitation production in our model.

Wang and Sobel [2012] performed a set of experiments that are similar to a subset of the experiments presented here. In that work, the authors simulated the response of convection to a layer of drying in the upper, middle, and lower troposphere. The drying represented horizontal advection of dry air, and the layer was relaxed to a water vapor mixing ratio of zero over a specified time scale. For drying, perturbations applied to the lower troposphere—at a level comparable to that used in this work—the moisture relaxation time scale varied from 2.9 to 100 days, and they noted that time scales below this range resulted in negative moisture values. The moisture relaxation time scale used in this work is shorter—1.8 days—but we are imposing a much weaker drying (or moistening) than in Wang and Sobel [2012], and are thus far from this numerical limitation.

Since our prognostic variable is θ_e rather than θ , our choices of moisture treatment also affect the sink of θ_e (and consequently moist entropy, see discussion after equation (10)):

$$S_e = w_{wtg} \frac{\partial \bar{\theta}_e}{\partial z} + \lambda_{adv} (\bar{\theta}_e - \theta_x) \frac{1}{\rho_0} \frac{\partial \rho_0 w_{wtg}}{\partial z} + \lambda_m (\bar{\theta}_e - \theta_{e0}), \quad (8)$$

where the overbar indicates the domain mean, θ_x is analogous to r_x , and θ_{e0} is the reference profile of equivalent potential temperature. Both θ_0 and r_{t0} (and thus θ_{e0}) can be functions of time to permit study of convection in time-dependent situations [e.g., Wang et al., 2013].

3.4. Multiple Equilibria

Multiple equilibria—steady states with either persistent precipitating deep convection or a completely dry troposphere—exist in WTG simulations with identical boundary conditions [Sobel et al., 2007; Sessions et al., 2010; Emanuel et al., 2013; Herman and Raymond, 2014]. If a set of parameters supports both equilibria, then whether the state is precipitating or dry depends on the initial moisture of the troposphere. We perform several multiple equilibria experiments to determine how the existence of multiple equilibria depends on the thermodynamic environment ($\theta_0(z)$, equation (3); $r_{t0}(z)$, equations (6) and (7)) and choice of moisture treatment.

As reported in Sessions et al. [2010], the model used here supports multiple equilibria for a range of wind speeds in conditions similar to those used in this work. Sessions et al. [2010] used unperturbed RCE reference profiles with laterally entrained moisture. A potentially significant difference, however, is that interactive radiation was used in the previous work; here, radiative cooling is static. Similar multiple equilibrium experiments were performed by Herman and Raymond [2014] on an updated version of this model with a modified WTG approach which spectrally decomposed the heating to accommodate gravity wave speeds representing a set of vertical modes. In a comparison of the “spectral WTG” approach with the conventional WTG (used in this study), multiple equilibria were found to exist only when conventional WTG was applied, and in that case, the range of multiple equilibria was sensitive to the choice of boundary layer height. We do not yet understand why conventional and spectral WTG give different results for multiple equilibria, though it may be related to the treatment of the boundary layer: in spectral WTG, convection confined to the boundary layer is shallow and thus has slow adjustment times [Bretherton and Smolarkiewicz, 1989]; in conventional WTG, this effect is artificially imposed via a linear interpolation of the WTG vertical velocity from the top of the boundary layer to zero at the surface (see discussion after equation (4)).

In another study, Anber et al. (“Effect of surface fluxes versus radiative cooling on tropical deep convection,” submitted to *Journal of the Atmospheric Sciences*, 2015) compared the existence of multiple equilibria in

WTG to an alternate parameterization of the large-scale (damped gravity wave, DGW; see Kuang [2008]; Blossey et al. [2009], for a description). In the parameter space they investigated, the WTG simulations exhibited multiple equilibria while DGW ones did not. Like spectral WTG, DGW does not require special treatment in the boundary layer, and the authors speculated that the existence of multiple equilibria may be an artifact of the boundary layer treatment when static radiation is used. Interactive radiation produced robust multiple equilibria in Sessions et al. [2010], so the role of radiation and boundary layer treatment is not entirely clear, and is left for future work.

The existence of multiple equilibria is sensitive to the method of parameterizing horizontal moisture advection. Sobel et al. [2007] demonstrated that multiple equilibria exist over a larger range of SSTs if horizontal moisture advection is not explicitly represented (equivalent to the control moisture treatment in this work) compared to when it is parameterized by moisture relaxation (see their Figure 2).

The first task is to determine whether multiple equilibria exist for an unperturbed environment using different moisture treatments. To test this, we simply run an experiment with a surface wind speed of 7 m s^{-1} and with zero initial moisture in the domain. We do this for each moisture treatment to determine how different parameterizations of horizontal moisture advection affect the existence of multiple equilibria. As in Sessions et al. [2010], for all experiments which exhibit multiple equilibria, we repeat with a surface wind speed of 10 m s^{-1} to determine the range over which multiple equilibria exist. We also repeat with a more stable and more moist environment to determine the role of the thermodynamic environment on multiple equilibria.

4. Diagnostics: Characterizing Convection and Its Environment

One of the most important measures of the strength of convection is the intensity of the precipitation it produces. The precipitation rate in itself—especially when averaged over space and time—is not enough to characterize the convection since different vertical and horizontal arrangements can produce the same mean precipitation rate. In order to better diagnose the convection, we compare the precipitation rates with several diagnostic quantities that we describe below.

The environmental stability is characterized by an instability index, Δs^* [Raymond et al., 2011; Gjorgjievska and Raymond, 2014], which is defined as

$$\Delta s^* = s_{low}^* - s_{high}^*, \tag{9}$$

where s^* is the saturated moist entropy, s_{low}^* is the mean saturated moist entropy in the level between 1 and 3 km, and s_{high}^* is the mean saturated moist entropy in the level between 5 and 7 km. Since s^* is a function of temperature and pressure only, this characterizes the stability of the environment: smaller values of the instability index correspond to more stable environments; larger values characterize more unstable environments.

The moisture content of the domain is characterized by the saturation fraction, which we approximate by

$$S = \frac{\int \rho(s - s_d) dz}{\int \rho(s^* - s_d) dz}, \tag{10}$$

where the integrals are taken over the entire vertical depth of the model, $s_d = c_p \ln(\theta/T_R)$ is the dry entropy ($c_p = 1005 \text{ J kg}^{-1} \text{ K}^{-1}$ is the specific heat at constant pressure, and $T_R = 300 \text{ K}$ is a constant reference temperature), and s is the moist entropy (with θ replaced by θ_e in the dry entropy definition).

We define deep convective inhibition (DCIN) as a measure of how conducive or hostile the environment is to convection. As in Raymond et al. [2003],

$$DCIN = s_t^* - s_b, \tag{11}$$

where the threshold entropy for convection, s_t^* , is the average saturated moist entropy over the layer between 1750 and 2000 m, and s_b is the boundary layer moist entropy, averaged over the lowest 1.75 km of the domain. Smaller or negative values of DCIN are conducive to developing deep convection; larger values inhibit it.

The normalized gross moist stability (NGMS) provides a measure of the response of convection to its environment [Neelin and Held, 1987]. It is typically defined as the export of some quantity that is approximately

conserved in moist processes (usually moist static energy or moist entropy) divided by some measure of the strength of the convection. As in *Raymond et al.* [2007], we choose NGMS (Γ) to be the ratio of moist entropy import to moisture export:

$$\Gamma = \frac{T_R [\nabla_h \cdot (\rho s \mathbf{v})]}{-L [\nabla_h \cdot (\rho r_t \mathbf{v})]} = \frac{T_R \int \nabla_h \cdot (\rho s \mathbf{v}) dz}{-L \int \nabla_h \cdot (\rho r_t \mathbf{v}) dz}. \tag{12}$$

The square brackets signify a vertical integral over the troposphere and ∇_h is the horizontal divergence operator. The reference temperature, T_R , and latent heats of condensation plus freezing, L ($L = 2.833 \times 10^6 \text{ J kg}^{-1}$), are included to make Γ dimensionless. Differing environmental profiles can significantly affect the value of Γ . Stabilizing or destabilizing the reference potential temperature will change the vertical profile of moist entropy which adjusts the lateral export of that quantity from the domain (numerator in equation (12)); drying or moistening the environment clearly affects the import of moisture into the domain (denominator in equation (12)), but it can also affect the amount of moist entropy exported or imported at given levels.

As in *Raymond et al.* [2007], we can relate the NGMS to the net precipitation rate in the steady state. To do this, we consider the vertically integrated conservation equation for specific moist entropy:

$$\frac{\partial [\rho s]}{\partial t} + [\nabla \cdot (\rho \mathbf{v} s)] = F_s - R, \tag{13}$$

which is the moist entropy analog of the vertical integral of equation (1). In this case, the advection term includes advection by the grid-scale and by the parameterized large-scale WTG velocity fields. F_s is the surface moist entropy flux due to surface heat and moisture fluxes, and R is the vertically integrated entropy sink per unit mass due to radiation. Similarly, vertically integrating equation (2) gives:

$$\frac{\partial [\rho r_t]}{\partial t} + [\nabla \cdot (\rho \mathbf{v} r_t)] = E - P, \tag{14}$$

where E is evaporation and P is precipitation, and the contribution by WTG circulations is included in the advection term on the left-hand side. In this work, we exclusively study the statistically steady state; setting the time derivatives in equations (13) and (14) to zero and substituting into equation (12) gives a relationship between NGMS and the net precipitation (precipitation, P , minus evaporation, E) [*Raymond et al.*, 2007]:

$$\Gamma = \frac{T_R (F_s - R)}{L (P - E)}. \tag{15}$$

Most of the experiments described hold the net entropy forcing constant: surface fluxes are fixed (F_s is constant) and a static radiative cooling profile implies R is constant. Thus, we expect $P - E \propto 1/\Gamma$, where the NGMS adjusts to account for the details of the thermodynamic environment.

We can infer much about the convective environment—as well as understand the relationship between our diagnostic quantities—by examining vertical profiles of mass flux. The vertical mass flux is calculated as the product of the density and the total vertical velocity. The total vertical velocity is the sum of the explicit velocity calculated by the model and the velocity field produced by enforcing WTG. Without WTG, mass conservation requires that the domain mean vertical velocity be zero (what comes up must go down), so the only domain mean vertical motion is that parameterized by the WTG approximation. Thus,

$$\text{mass flux} = \rho w_{wtg}. \tag{16}$$

5. Results

In this section, we show the time evolution of precipitation and the diagnostic quantities defined in section 4 to demonstrate the effect of changes in the thermodynamic environment. We also present vertical profiles of potential temperature and moisture anomalies to compare with the imposed anomalies. Vertical profiles of mass flux demonstrate how convection develops as a function of changes in the thermodynamic environment and parameterization of horizontal moisture advection. Finally, we compare steady state values of precipitation and the diagnostic quantities defined in section 4 in a set of scatter-plots to characterize the response of convection to changes in the large-scale thermodynamic environment.

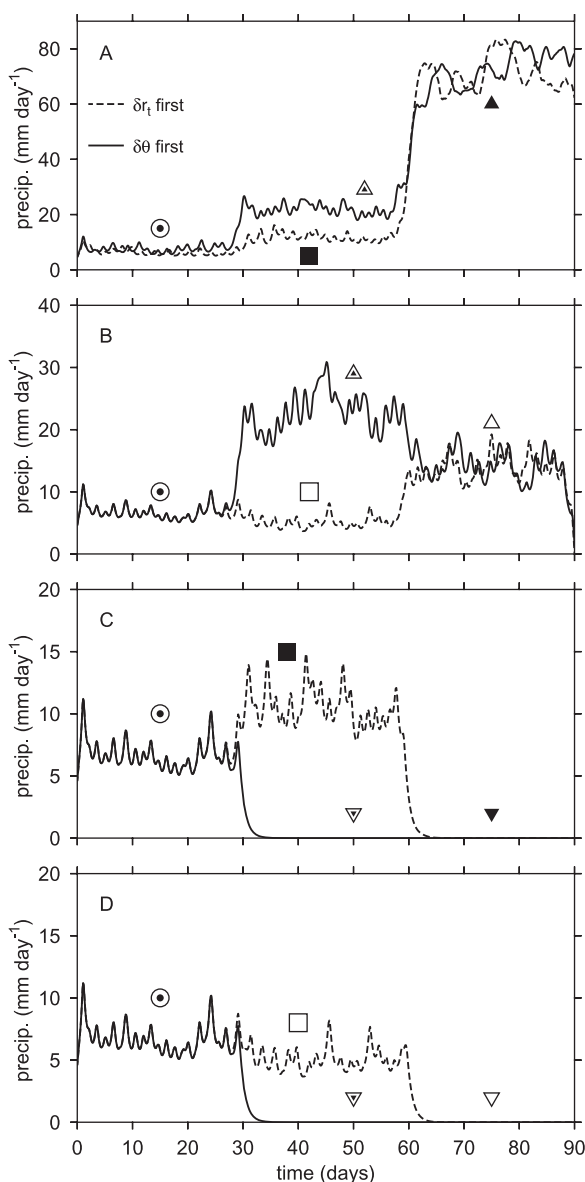


Figure 6. Three month time series of precipitation rate for the eight WTG experiments graphically described in Figure 4. (a) Experiments 1 and 2; (b) experiments 3 and 4; (c) experiments 5 and 6; and (d) experiments 7 and 8. The symbols indicate the perturbations of the reference profile for the 1 month segment, the symbol legend is given in Figure 3. Solid and dashed lines indicate whether the reference θ or reference r_t profiles, respectively, were perturbed first (these indicate the perturbed profile during the second month of the experiments). Data in this figure have been low-pass filtered in time with a cut off period of 1 day.

1. The increase in stability—cooling of 2 K at low levels and warming of 2 K aloft—produces a larger increase in precipitation rate (21 mm d^{-1}) than a 1 g kg^{-1} increase in atmospheric moisture of (12 mm d^{-1}); see the second month in Figure 6a.
2. Decreasing the moisture by 1 g kg^{-1} at 3 km reduces—but does not shut off—the precipitation; whereas destabilizing the environment completely shuts off the convection, even in a moister environment (compare empty squares in Figures 6b and 6d with inverted triangles in Figures 6c and 6d).
3. A drier, more stable environment increases the precipitation rate compared to the unperturbed RCE profile, whereas the moister, less stable environment is completely devoid of precipitation (compare the third month in Figures 6b and 6c).

These observations are specific to the magnitudes of perturbations applied to the reference profiles, though different choices would likely give qualitatively similar results. It would be interesting to investigate how

5.1. Response to Changes in the Thermodynamic Environment for Laterally Entrained Moisture

In this section, we analyze the time dependence of the diagnostic quantities defined in section 4. We note that all figures showing time series data have been low-pass filtered in time with a cut off period of 1 day.

Figure 6 shows a time series of the precipitation rate for the experiments outlined in Figure 4. For convenience, we only show the time series for moisture that is parameterized by lateral entrainment ($\lambda_{hadv}=1, \lambda_m=0$ in equation (6)); similar results hold for other moisture advection choices, but are not shown. All simulations use unperturbed RCE profiles during the first month; each of the four plots represents the four possible combinations of reference profiles when both θ and r_t are perturbed; the second month in each case represents either a drying/moistening OR a stabilizing/destabilizing. Each case is marked with the symbol given in Figure 3. Each distinct combination of reference profiles (each plot in Figure 3) is repeated at least twice (see Figure 4). Statistics for similar conditions are comparable, indicating statistically identical steady states.

For the perturbation magnitudes used in this study, atmospheric stability predominately affects the character of convection compared to atmospheric moisture. Specifically:

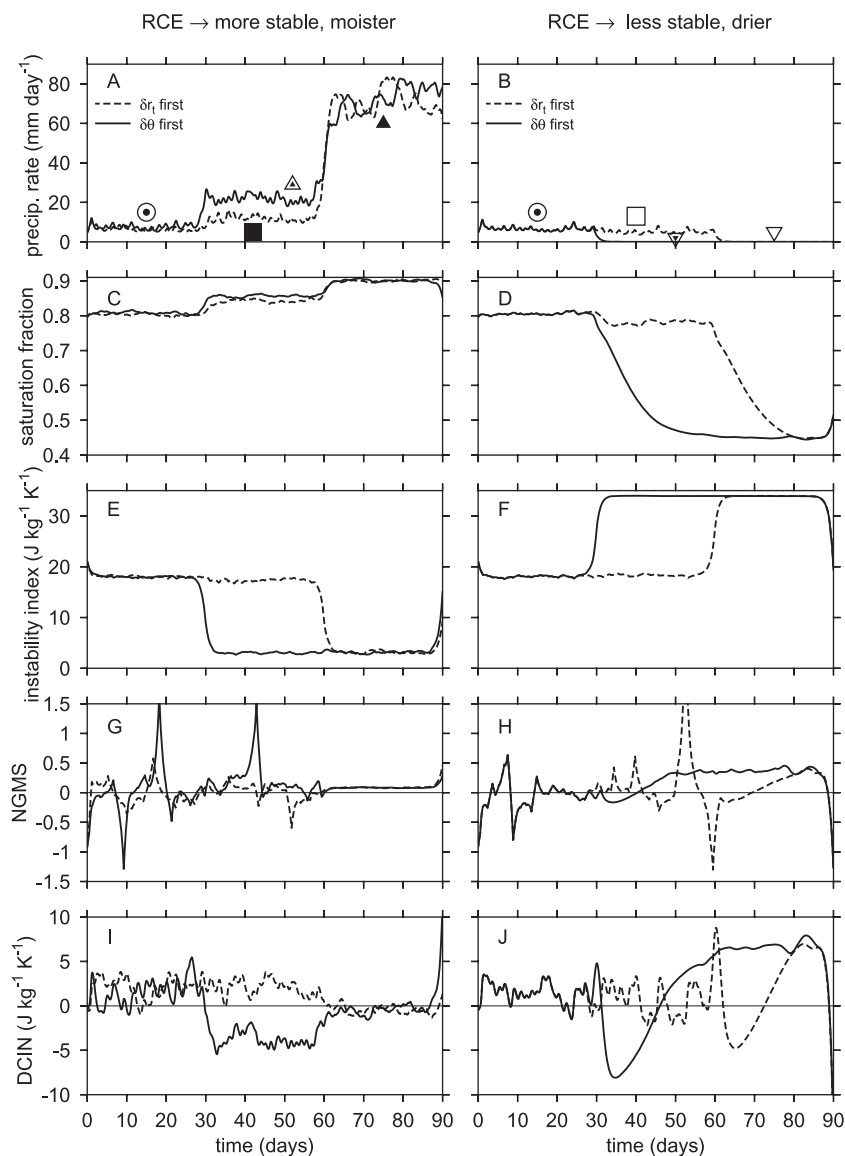


Figure 7. Time series showing precipitation rate (a,b), saturation fraction (c,d), instability index (e,f), NGMS (g,h), and DCIN (i,j) for experiments which became more stable and moister (left column, experiments 1 and 2 in Figure 4), and those which became less stable and drier (right column, experiments 7 and 8 in Figure 4). Data in this figure have been low-pass filtered in time with a cut off period of 1 day.

different magnitudes of drying and moistening or stabilizing and destabilizing would affect the precipitation rate. Wang and Sobel [2012] performed a series of WTG experiments to see the effect that drying a layer would have on convection. In the lowest drying layer—comparable to the level that moisture perturbations are applied to in these experiments—relaxing the moisture to 0% relative humidity still produced convection with nonzero precipitation (though the convection became strictly shallow). Thus, we do not expect moisture perturbations to have as dramatic effects as perturbations in potential temperature.

In addition to precipitation rate, we consider several other diagnostic variables for characterizing convection and its environment. To develop some intuition about how these diagnostics behave for different convective environments, Figure 7 shows time series of precipitation rate, saturation fraction, instability index, NGMS, and DCIN (these are all defined in section 4). The left column shows the results for the experiments which became more stable and more moist (experiments 1 and 2 in Figure 4, Figure 6a); while those on the right column evolve to less stable and drier states (experiments 7 and 8 in Figure 4; Figure 6d). The vertical axes were chosen to be the same for both columns for easy comparison. As in Figure 6, horizontal moisture advection is parameterized using lateral entrainment.

From Figure 7, we note several features of the diagnostic quantities. First, saturation fraction seems to adjust relatively quickly to changes in moisture and to an increase in stability, but it takes the domain a long time to adjust to a decrease in stability (Figure 7d). The slow adjustment is primarily due to the relatively slow radiatively driven subsidence rate, which determines the steady state in absence of active convection. This only happens when horizontal moisture advection is parameterized using lateral entrainment for reasons described later in this section. Because we calculate mean quantities from the last 2 weeks of each month long segment, the long adjustment time for saturation fraction does not give the actual equilibrium value for the statistics calculated in this work. However, the error in the mean is much smaller than the difference between saturation fraction values for precipitating and nonprecipitating states, so we simply make note of the difference and interpret the diagnostics accordingly.

The instability index—shown in Figures 7e and 7f—is calculated from the saturated entropy. Since this is constrained by the enforcement of WTG, it quantifies “more stable” (small values) and “less stable” (large values) environments. It adjusts quickly to changes in θ profiles, but is not sensitive to changes in the reference moisture profile.

Depending on the atmospheric conditions, NGMS can be a highly variable quantity (Figures 7g and 7h). It is defined as the ratio of lateral moist entropy export to lateral moisture import (equation (12)). As convection evolves in the domain, these quantities can alternate between import and export. This is especially true if conditions are close to RCE: since the system is nearly in balance, there should be no net lateral import and export from the domain and these quantities alternate across the zero value. This results in large fluctuations, and in these conditions, NGMS is not a good diagnostic quantity. Because our simulations are performed in two-dimensions, there is more intermittency in convection which results in greater fluctuations between import and export compared to three dimensions [Wang and Sobel, 2011]. Even in a more stable environment (days 30–60 in Figure 7g) where moisture import exceeds export, convection is intermittent and significant fluctuations generate considerable variability in NGMS. On the other hand, for conditions which are not close to RCE—when either import or export is dominant—NGMS provides important information about the relationship between convection and the convective forcing. For example, the last month in Figures 7g and 7h show steady, positive values of NGMS. In the more stable case with nonzero precipitation (Figure 7g), the domain is importing moisture and exporting moist entropy, and the precipitation rate is related to the value of NGMS according to equation (15). In the less stable environment (Figure 7h), precipitation is suppressed, moisture is exported from the domain, and there is weak import of moist entropy. This is explained in more detail in section 5.3.

We can gain considerable insight to the response of convection to different thermodynamic environments by understanding the behavior of DCIN. Figures 7i and 7j shows the time evolution of DCIN, and Figure 8 also shows the time series of the components of DCIN: the threshold saturated moist entropy (s_t^*) is shown in red, the boundary layer moist entropy (s_b) is in blue. These are plotted for the experiments where the θ profile is perturbed first (solid lines in Figures 8c and 8d), and the r_t profile is perturbed first (dotted line in Figures 8e and 8f). There are three important observations:

1. Moisture perturbations have very little impact on either s_t^* or s_b (with the exception of increasing s_t^* in a more stable environment as seen at day 60 in Figure 8c). This makes sense since s_t^* is a function only of temperature, and although WTG is not directly enforced in the boundary layer, s_b is more sensitive to $\theta_{ref}(z)$ than $r_{t,ref}(z)$ (see Figures 9 and 10); boundary layer anomalies are fairly uniform in different moisture environments but are strong functions of stability. The boundary layer is drier in a more stable environment and moister in a less stable one.
2. Changing atmospheric stability affects both s_t^* and s_b , so the significant variations in DCIN are related to the direct change in s_t^* (which is calculated near the level of the perturbation) and an indirect change in moisture.
3. s_t^* and s_b rapidly adjust to changes in the reference potential temperature profile with one important exception: the boundary layer moist entropy, s_b , exhibits a very slow response to a decrease in atmospheric stability.

The last observation deserves some explanation. Recall that s_b is the mean moist entropy in the lowest 1.75 km—which includes a thin layer just above the 1 km nominal boundary layer. Immediately following the decrease in stability, DCIN increases trivially (Figure 8b, DCIN has a maximum of about $5 \text{ J kg}^{-1} \text{ K}^{-1}$ at day

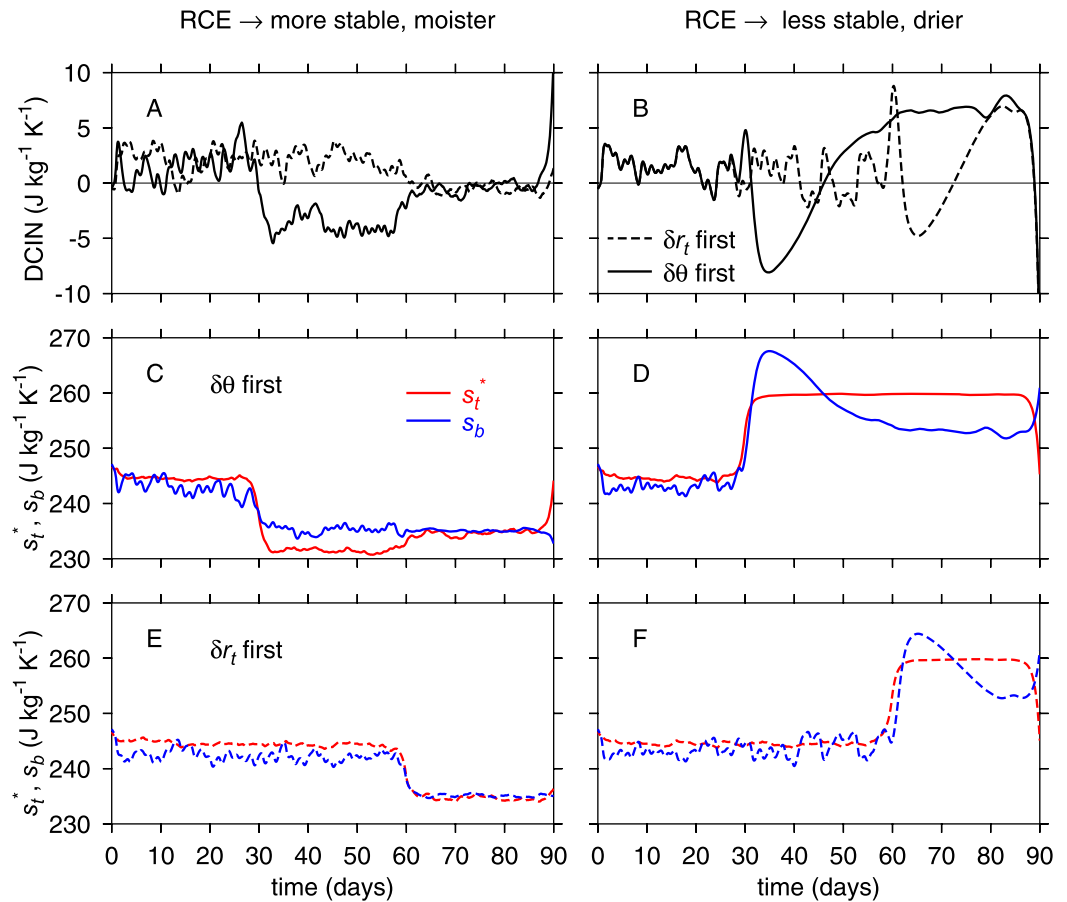


Figure 8. Time series of DCIN (a,b), and DCIN components, s_t^* and s_b (c-f). The solid lines represent experiments where the θ profile was perturbed first (c,d), while dashed lines represent experiments where moisture perturbations are imposed first (e,f). As in Figure 7, the left column represents experiments 1 and 2 while the right column shows results for experiments 7 and 8 (see Figure 4). Data in this figure have been low-pass filtered in time with a cut off period of 1 day.

30) as a result of the rapid increase in s_t^* (the response time is less than a day, and is noted by the slight lead in increase in s_t^* compared to s_b at day 30 in Figure 8d). After the initial increase, DCIN decreases sharply over a period of about 3 days; boundary layer fluxes rapidly increase s_b . This is because deep convection is suppressed due to the stable layer in the lower troposphere. Surface fluxes eventually reach a steady state while radiatively driven subsidence continues to stifle convection of surface parcels and even acts to reduce boundary layer entropy. This occurs over a period of about 25 days, after which DCIN finally reaches a steady state. This mechanism also explains the gradual decline in saturation fraction in Figure 7.

It is important to note that this slow response only occurs when lateral entrainment is the choice for moisture treatment ($\lambda_{adv}=1, \lambda_m=0$); all other choices result in a rapid adjustment to any change in the thermodynamic environment (not shown). The long adjustment time for the lateral entrainment only treatment is likely a result of the linear interpolation of the WTG vertical velocity to zero in the boundary layer (first two terms in the right-hand side of equations (6) and (8)). This constraint implies that lateral entrainment vanishes near the surface, so boundary layer entropy may only be reduced by slower subsidence processes. When lateral entrainment is turned off ($\lambda_{adv}=0$), or when moisture relaxation is turned on ($\lambda_m \neq 0$), the boundary layer entropy can quickly adjust to the reference profile, thus reducing the transition time.

5.2. Vertical Profiles

In order to interpret the mean diagnostics, it is helpful to compare vertical profiles of θ and r_t perturbations to the imposed perturbations; it is also useful to analyze the vertical motion that arises as a consequence of these anomalies and of the different parameterizations for horizontal moisture advection. It is important to note that the vertical resolution throughout the troposphere—including the boundary layer—is 250 m.

Table 1. Abbreviations for the Different Combinations of Moisture Treatment^a

	$\lambda_{hadv}=0$	$\lambda_{hadv}=1$
$\lambda_m=0$	control	lat ent
$\lambda_m=1/1.8 \text{ d}^{-1}$	m-relax	both

^aThe values of λ_{hadv} and λ_m (equation (6)) determine the choice for parameterizing horizontal moisture advection. This is the key for identifying each method: lateral entrainment (lat ent), moisture relaxation (m relax), both (lat ent and m relax). Choosing $\lambda_{hadv}=\lambda_m=0$ disconnects the modeled convection from the reference moisture profile; this is the control.

While this is sufficient for most of the troposphere, it is too coarse for the boundary layer and thus limits the extent to which we can make physical interpretations about the behavior in the boundary layer. Nevertheless, it is useful for making qualitative comparisons and explaining the response of convection to different thermodynamic environments.

As discussed in section 3.3, the choices for parameterizing horizontal moisture advection are entirely captured in the values for λ_{hadv} and λ_m in

equation (6). Table 1 summarizes the values used in this study and identifies the abbreviations used for the results of this section.

We expect the θ profile to be very close to the reference profile—independent of the moisture treatment—simply as a consequence of enforcing the WTG approximation (see equation (3)). Figure 9 shows that this is indeed the case: the model's θ anomalies are very close to the imposed profiles, with the exception of the boundary layer where WTG is not enforced. The largest deviation from the free tropospheric reference

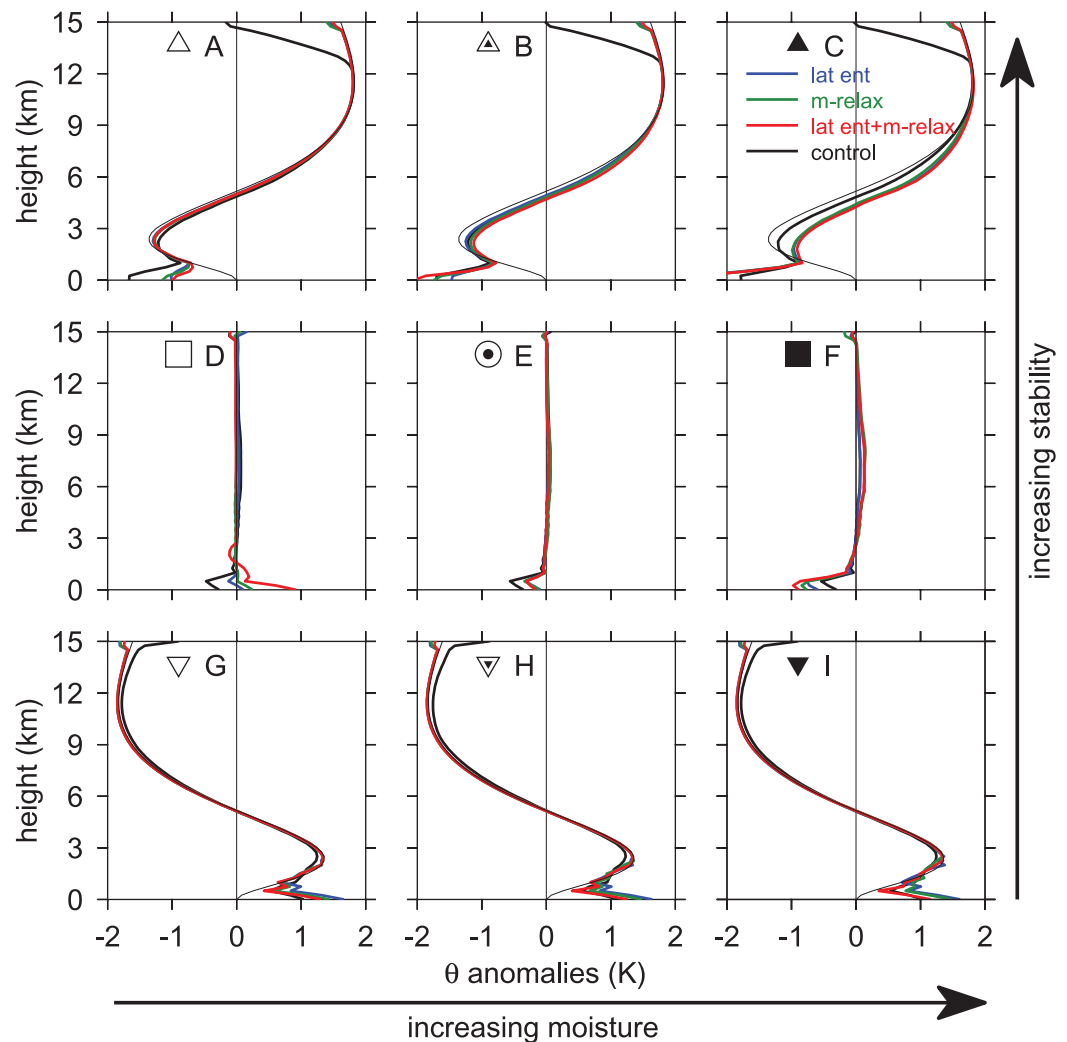


Figure 9. Modeled θ anomalies for each distinct thermodynamic environment (represented symbolically as in Figure 3). Colors represent moisture treatment: lateral entrainment is blue; moisture relaxation is green; red uses both lateral entrainment and moisture relaxation; and black uses neither. For reference, the thin black lines show the anomalies imposed on the reference profile (see Figure 3).

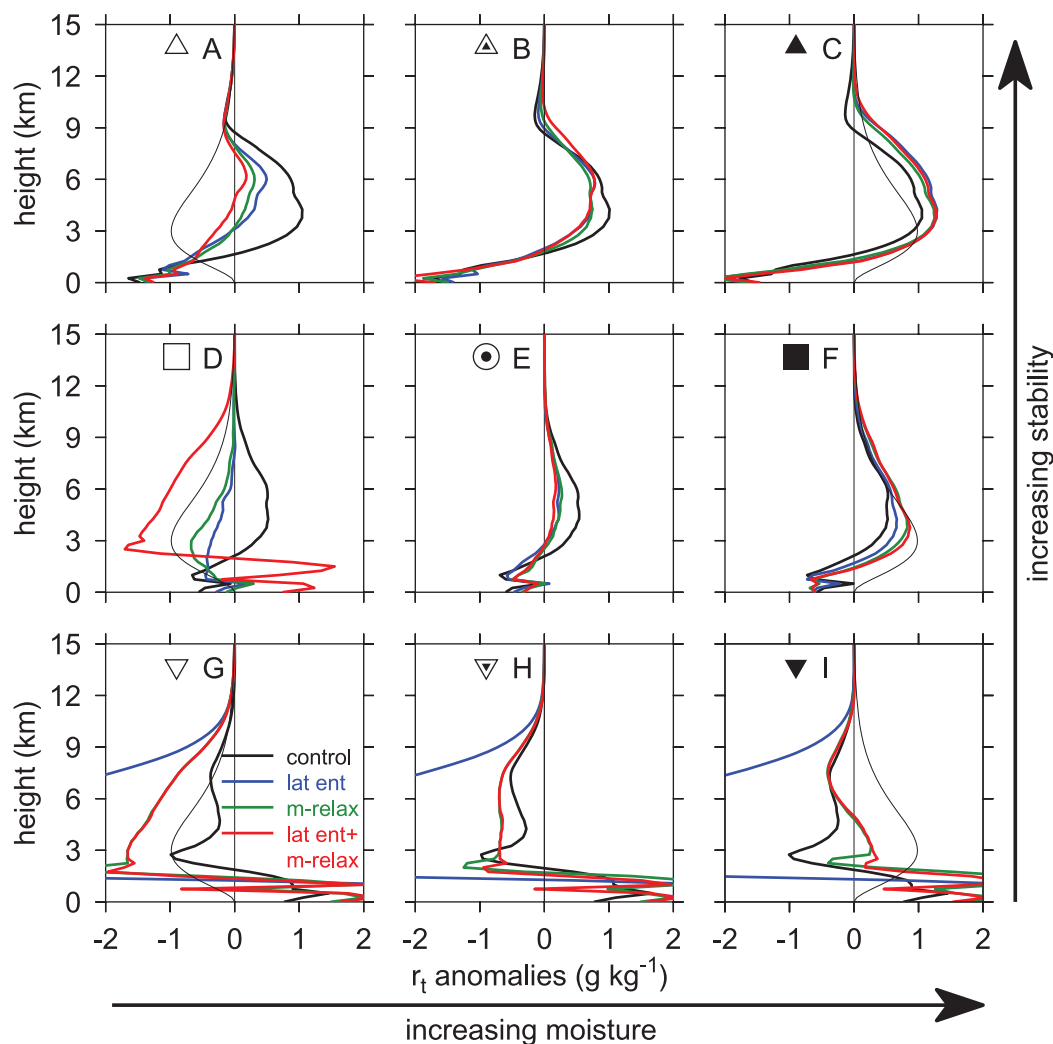


Figure 10. Moisture anomalies for different thermodynamic environments using different moisture treatments (denoted by color; see Table 1 for a legend of abbreviations). The thin black line shows the imposed moisture perturbation for reference (same as Figure 3). The dry anomaly for lateral entrainment (blue) in Figures 10g–10i has a minimum value of nearly -9 g kg^{-1} at an altitude of about 2 km.

profile occurs in the environment which is both moister and more stable (Figure 9c); the domain mean is slightly warmer in the lower troposphere, and the effect is slightly exaggerated in all cases where horizontal moisture advection is explicitly parameterized.

In contrast, there are significant differences in the moisture anomalies generated by the model compared to the imposed anomalies in the reference profile. A careful comparison of the moisture anomalies in Figure 10 for each distinct environment suggests that the reference moisture seems to play a supporting role for the convection rather than a dominant one. This is illustrated by noting that the shape of the moisture anomalies are more consistent with the perturbations applied to the θ profiles than to the moisture profiles. For example, in the control case where moisture is only advected vertically ($\lambda_{adv} = \lambda_m = 0$), there is no sensitivity to changes in the reference moisture profiles—by design—but there is dependence on the stability of the reference θ profile. The stronger dependence on environmental stability is also seen when horizontal moisture advection is parameterized; for example, Figures 10a–10c (top row)—corresponding to more stable environments—show more moist middle tropospheres, even in a drier environment. In these cases, the lowest few kilometers are significantly drier, which is likely a consequence of weak descent in that layer (as seen in the vertical mass flux, Figures 11a–11c).

An important observation is that less stable environments (Figures 10g–10i) produce drier free tropospheres, even if the environment itself is moister (Figure 10i). This is especially true if horizontal moisture

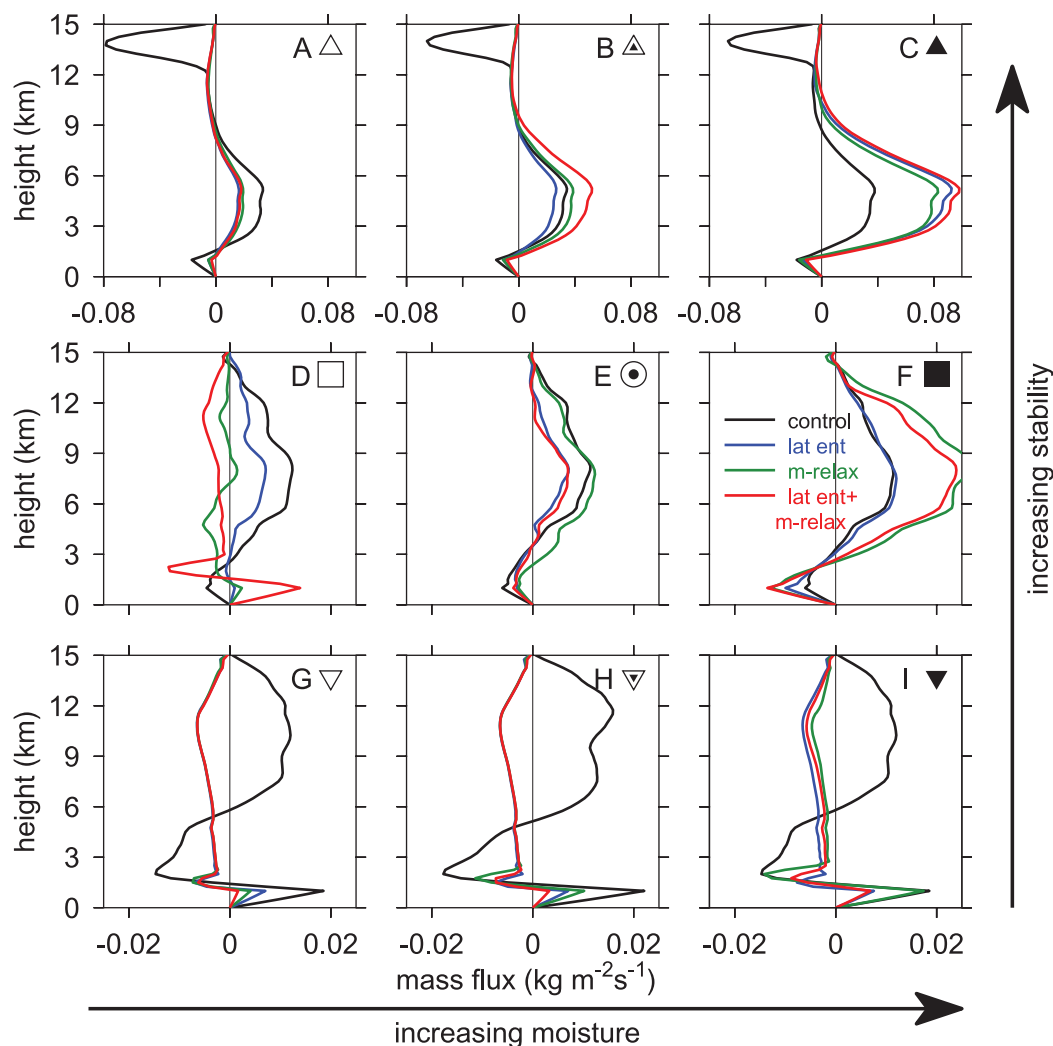


Figure 11. Vertical profiles of vertical mass flux (equation (16)) for each environmental profile. Colors represent the moisture treatment used. Note the different horizontal scale in the top row figures compared to the other rows. Each tick mark on the horizontal axes in the top row represents $0.04 \text{ kg m}^{-2}\text{s}^{-1}$, while those in the middle and bottom rows represent $0.02 \text{ kg m}^{-2}\text{s}^{-1}$. More stable environments exhibit much stronger vertical mass fluxes.

advection is parameterized by lateral entrainment. In this case, radiatively driven subsidence results in an extremely dry anomaly—up to -9 g kg^{-1} —at an altitude of 2 km. No other moisture treatment reduces the tropospheric moisture by this amount.

When used simultaneously, moisture relaxation and lateral entrainment usually work together to contribute either to an overall drying or moistening of the environment. An exception occurs in a less stable environment. In this case, lateral entrainment contributes to an extreme drying compared to the other parameterizations; when used in combination with moisture relaxation, the reference profile is moister than the domain mean vertical moisture profile, and the relaxation counters the extreme drying that occurs when lateral entrainment is used exclusively.

Comparing vertical mass flux profiles for the different moisture treatments in different environments can shed light on the behavior of convection in these simulations. With a few exceptions, the most important factor in determining the shape of the vertical mass flux profile is environmental stability. Changing the reference moisture primarily modulates the magnitude of the mass flux profile, but does not change the shape. This is in contrast to results presented by Wang and Sobel [2012] who found that extreme drying of a layer in the lower troposphere prevents deep convection altogether.

More stable environments— independent of moisture or moisture treatment— have stronger, more “bottom-heavy” convective profiles than unperturbed or less stable environments (compare rows in Figure 11). Conceptually, we can visualize buoyant parcels accelerating faster in the low-level cool anomaly, and becoming less buoyant in the warm anomaly aloft, thus producing a bottom-heavy profile. This is supported by the results of *Bretherton and Smolarkiewicz* [1989]. On the other hand, less stable environments inhibit convective development; consequently, radiative cooling produces subsidence throughout the free troposphere, though weak updrafts persist in the boundary layer. Environments with decreased stability effectively suppress convection— independent of the environmental moisture— with one exception: If horizontal moisture advection is turned off so that moisture transport within the domain is dominated by vertical advection (control case, black line), there is upward motion above 5 km, with slightly stronger descent between the boundary layer and 5 km. In this case, the cooling aloft accelerates the buoyant parcels upward while the warm anomaly below results in descent. This strict response to changes in the atmospheric stability is modified significantly if horizontal moisture advection is explicitly parameterized and environmental moisture is permitted to enter the domain. In this case, drier environmental air (represented by the reference profile) inhibits condensation of lifted moisture— and evaporates any condensation— which cools the parcel and results in descent. The overturning of boundary layer air, necessitated by surface fluxes, is amplified by moister environmental air so this effect monotonically increases with the amplitude of the imposed moisture anomaly (Figures 11g–11i).

The most significant difference in mass flux profiles when comparing different parameterizations of horizontal moisture advection occurs in less stable (nonprecipitating) environments: the mass flux profile differs significantly when horizontal advection is not explicitly parameterized (control) compared to when it is (via lateral entrainment and/or moisture relaxation). Aside from this, there are not many significant qualitative differences in mass flux profiles for different moisture treatments with one exception: in the absence of θ -perturbations, the convection is more sensitive to the choice for parameterizing moisture advection, especially in a dry environment (see Figure 11d). In this case, there is almost no vertical motion if moisture relaxation is used (green line); weak upward motion develops if moisture is laterally entrained (blue); but there is weak descent if both mechanisms are employed (red). The moisture relaxation case is consistent with the findings of *Wang and Sobel* [2012].

5.3. Diagnosing Convection

Now that we have some insight as to how the shape and strength of convection depends on atmospheric stability, environmental moisture, and choice for parameterizing horizontal moisture advection, we investigate the relationship between precipitation and the diagnostic quantities defined in section 4. This allows us to quantify the impact of the thermodynamic environment on the convection itself. Figure 12 shows scatter plots of rain as a function of saturation fraction, instability index, NGMS, and DCIN. Each symbol represents time and domain averages of the last 2 weeks (minus 1 h to avoid the ambiguous data at the transition) of each 1 month segment of the simulations. The symbols themselves identify the reference environment— the environmental moisture and stability— according to the legend embedded in the top left plot (this symbol-only legend corresponds to the perturbations shown in Figure 3). Colors indicate moisture treatment used; Table 1 gives a simple legend for abbreviations and gives the values of λ_{hadv} and λ_m which determine the moisture treatment according to equation (6).

There are several observations to make from Figure 12. First, consistent with observations [*Bretherton et al.*, 2004; *Peters and Neelin*, 2006; *Masunaga*, 2012; *Gjorgjievska and Raymond*, 2014] and other modeling studies [*Derbyshire et al.*, 2004; *Sobel and Bellon*, 2009; *Wang and Sobel*, 2012], we see that precipitation is a strong function of saturation fraction and instability index (Figures 12a and 12b). More moist and more stable environments— as indicated with smaller instability indices, higher saturation fractions, and filled upright triangles— produce the highest precipitation rates. The former is expected; the latter is a consequence of the bottom-heavy convective profile associated with more stable environments (Figure 11). The bottom-heavy convection vertically advects moister low-level air which increases the precipitation efficiency, even in drier environments. This effect is enhanced in simulations with explicit lateral moisture entrainment, where $\lambda_{hadv} = 1$ and $\lambda_m = 0$ (blue), and $\lambda_{hadv} = 1$ and $\lambda_m = 1$ (red).

Less stable environments— as indicated with inverted triangles— inhibit precipitation in most cases (Figure 12b; the exception being the control moisture treatment, $\lambda_{hadv} = \lambda_m = 0$); they have lower saturation fractions

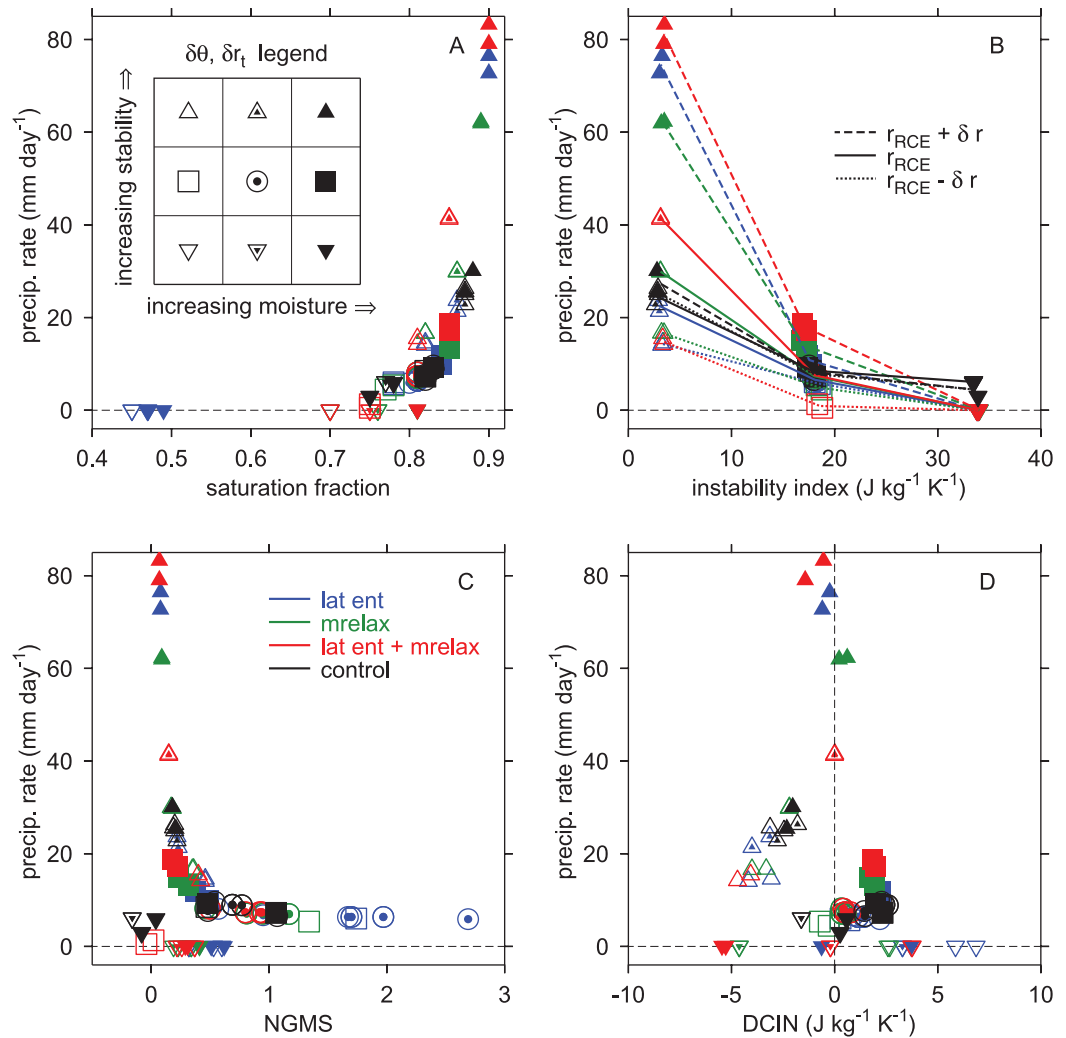


Figure 12. Scatterplots of precipitation as a function of (a) saturation fraction, (b) instability index, (c) NGMS, and (d) DCIN. Each shape represents a domain and time average for a given set of environmental conditions (see legend inset in Figure 12a, and corresponding perturbations in Figure 3). Colors represent parameterization choices for horizontal moisture advection according to Table 1: blue indicates explicit lateral entrainment; green is moisture relaxation; red indicates both are used; and black is the control (no explicit parameterization). The lines in Figure 12b connect experiments with identical reference moisture profiles: solid lines have unperturbed moisture profiles (r_{RCE}), dashed are more moist ($r_{RCE} + \delta r$), dotted are drier ($r_{RCE} - \delta r$).

and higher values of DCIN (Figures 12a and 12d, respectively). The warm anomalies in the lower troposphere inhibit moist parcel ascent in general, and result in negative vertical mass fluxes throughout the troposphere. Note the extremely low saturation fractions observed with lateral entrainment (blue symbols in Figure 12a). In this case, radiatively driven subsidence down the moisture gradient with no source of moisture to offset the drying (either explicitly via moisture relaxation or implicitly at entraining levels as in the control case, Figures 11g—11i) results in severe drying of the troposphere (Figures 10g—10i). This has important consequences for multiple equilibria—and convective self-aggregation—as discussed in section 5.4.

There are a few cases where there is no precipitation despite having saturation fractions above 0.7; this occurs in a less stable environment when moisture relaxation is applied, either as the only treatment or in conjunction with lateral entrainment (Figure 12a). In this case, moisture relaxation is moistening a 5 km layer above the surface (with heavy moistening in the boundary layer, see Figures 10g—10i) which results in a relatively high value of saturation fraction. However, the temperature anomalies are still generating descent throughout the free troposphere which inhibits precipitation (compare mass flux profiles in Figures 11h and 11i).

According to equation (15), static radiative cooling rates and fixed surfaces fluxes should produce an inversely proportional relationship between precipitation and NGMS. Figure 12c demonstrates this beautifully

for all moisture treatments with nonzero precipitation rates. We should note that NGMS is a poor diagnostic in conditions close to RCE since the system is nearly in balance and the net import/export of moisture and moist entropy is near zero, resulting in large variations in NGMS as a result of averaging zero over zero (in these simulations, values of $NGMS > 1$ represent poor diagnostic values). Nonprecipitating simulations all have small values of NGMS. In these cases, moisture is exported from the system while moist entropy is weakly imported due to circulations in the boundary layer. Note that there are several black symbols (control simulations) with negative values of NGMS. These simulations do not explicitly parameterize horizontal moisture advection ($\lambda_{hadv} = \lambda_m = 0$)—the convection is insensitive to the reference moisture profile—and, as discussed in the previous section, they exhibit a drastically different convective profile compared to the other moisture treatments in unstable environments (Figures 11g—11i). Rather than descent through the entire free troposphere, there is ascent from 6 km to the tropopause which vertically advects moisture and produces a nonzero precipitation rate. In terms of the contribution to NGMS, however, the vertical motion in the lower troposphere—descent in the boundary layer and ascent between the top of the boundary layer and 5 km—gives net import (sources) of both moisture and moist entropy, which results in $NGMS < 0$.

More stable environments exhibit small or negative values of DCIN, and thus represent thermodynamic conditions most conducive for developing deep convection. We expect unstable environments to be associated with larger DCIN; this is the case for some experiments (Figure 12d), though some show negative DCIN despite descent through the free troposphere (compare Figures 11g—11i). These cases have more moisture in the layer below 1.75 km as a consequence of relaxing the domain mean moisture profile to the reference profile; this increases s_b and thus decreases DCIN in these cases.

It is interesting that the highest precipitation rates do not occur for the most negative values of DCIN, but rather for values that are near zero. We can understand this behavior by reexamining Figures 7a, 7i and 8a, 8c. If the environment becomes more stable (e.g., day 30 in Figure 8c), both s_t^* and s_b decrease as a direct consequence of the applied cooling in the lower troposphere; this has a greater effect on s_t^* , which results in a negative DCIN (indicating an environment conducive to developing deep convection, see discussion in section 5.1). When moisture is then added to the lower troposphere (day 60 in Figure 8c), s_t^* increases slightly and DCIN becomes approximately zero (Figures 8a, 8c, and 12d). One possible explanation for the increase in s_t^* is that a more moist environment will entrain less dry air which results in less evaporative cooling, and a slightly higher temperature. In contrast, a drier environment will experience more evaporative cooling and more negative DCIN values (compare empty and filled upright triangles in Figure 12d). Since DCIN is approximately equal to negative lower tropospheric convective available potential energy (CAPE), dry parcels require more negative values of DCIN to ascend.

We can further understand the factors controlling the characteristics of convection by considering relationships between the diagnostic quantities themselves. Figure 13 shows scatter plots which compare saturation fraction, instability index, NGMS, and DCIN.

Figure 13a clearly demonstrates that the more stable the environment, the higher the saturation fraction (this is consistent with results of Gjorgjievska and Raymond [2014]). For a given reference moisture profile (denoted by line style), the relationship is nearly linear for most moisture treatments. The exception to this is the extreme drying in unstable environments when horizontal moisture advection is parameterized by lateral entrainment. This reinforces the notion that the important difference between moisture treatments is not what happens when it is precipitating (precipitation rates and mass flux profiles are fairly consistent), but what happens to the domain when it is not precipitating. This may be especially relevant for interpreting results of WTG simulations which impose observed data in time-dependent reference profiles, or for understanding conditions permitting multiple equilibria.

Figure 13b shows the relationship between saturation fraction and NGMS. For precipitating environments in conditions where NGMS is a good diagnostic, smaller values of NGMS correlate to larger saturation fractions (see inset, Figure 13b), which is consistent with the precipitation-NGMS relation of Figure 12. In nonprecipitating cases, NGMS is small as a consequence of weak import (or export) of moist entropy near the top of the boundary layer.

There is not a significant relationship between NGMS and DCIN (Figure 13c). This is an interesting result that is consistent with the theories posited by Raymond and Fuchs [2007] and Raymond and Fuchs [2009]. Together, these papers developed a highly simplified model of the interaction between the large-scale and tropical

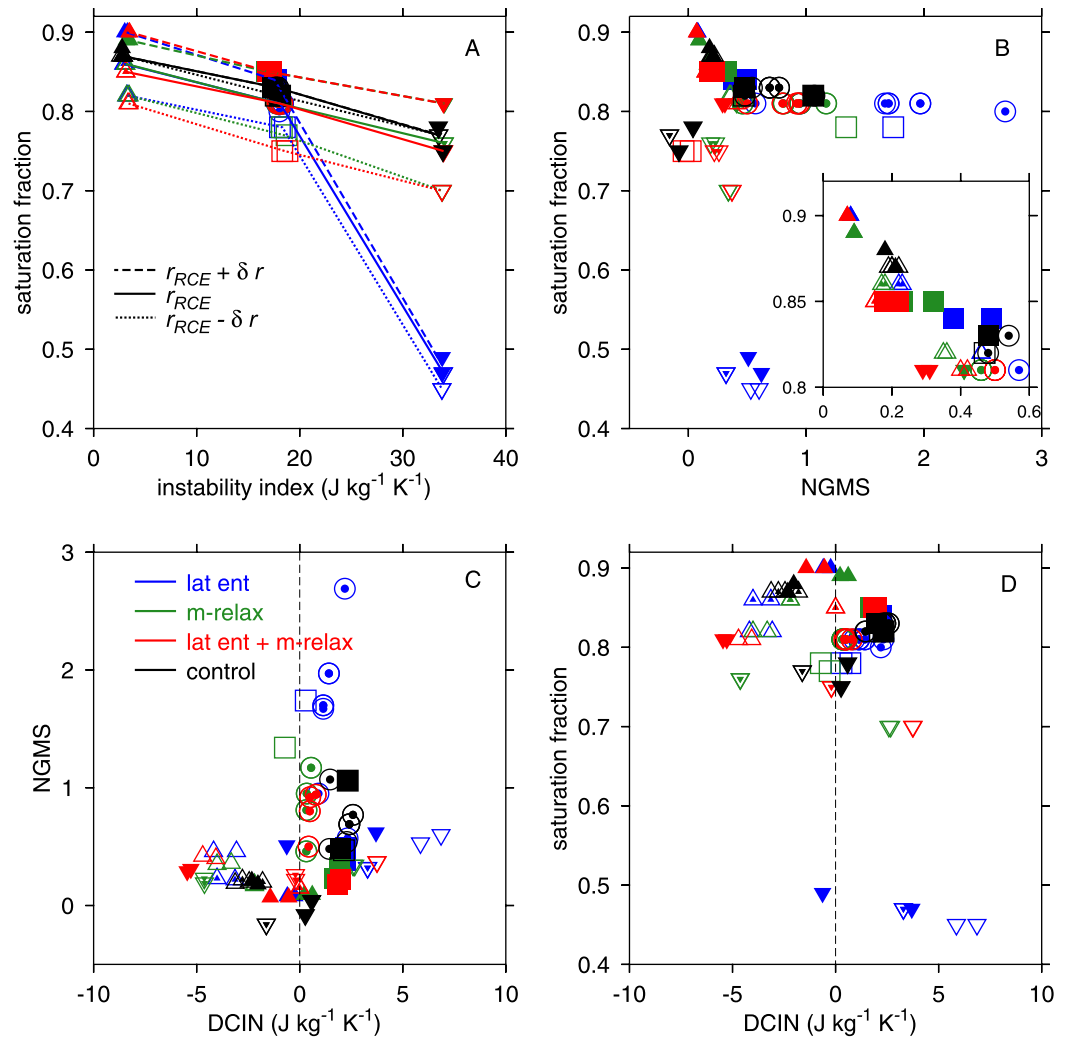


Figure 13. Relationships between diagnostic quantities: (a) saturation fraction versus instability index, (b) saturation fraction versus NGMS, (c) NGMS versus DCIN, and (d) saturation fraction versus DCIN. Colors indicate choice for horizontal moisture advection, while shapes indicate environmental stability and moisture according to the symbol legend defined in Figure 12. Note the strong relationship between saturation fraction and instability index. As in Figure 12, lines in Figure 13a connect experiments with identical reference moisture profiles.

oceanic convection. Their analytic model identifies two types of convectively coupled waves: moisture modes in which convection acts to increase—rather than decrease—the saturation fraction (this happens when NGMS is negative), and another mode which is destabilized by convective inhibition. An example of the latter is convectively coupled Kelvin waves, and recent modeling results by *Fuchs et al.* [2014] demonstrated the role of DCIN in destabilizing the two-dimensional analog of convectively coupled Kelvin waves. This simplified picture suggests that either NGMS or DCIN is the control for destabilizing the environment, depending on the nature of the interaction between convection and the large-scale. In reality, the dynamic processes are much more complicated due to the inherent nonlinearity of the atmosphere, so we do not expect an obvious relation between NGMS and DCIN, despite good correlations between other convective diagnostics.

Similarly, there is also no obvious overall correlation between DCIN and saturation fraction (Figure 13d). Here, the primary observation is that more stable environments—upright triangles—experience small or negative DCIN, which is indicative of an environment conducive to convection. As explained above, DCIN in these environments becomes less negative for more moist environments (indicated with filled upright triangles and higher saturation fractions) because less dry air is entrained, evaporative cooling is diminished, and the threshold entropy increases. Also noteworthy is that the highest values of DCIN accompany the lowest saturation fractions, and these occur only with laterally entrained moisture, and only in the most hostile environment for convection: more unstable and drier.

To summarize Figures 12 and 13, we note the following features:

1. The precipitation rate is highly sensitive to both the saturation fraction and the atmospheric stability (as measured by the instability index).
2. Stable environments are conducive to precipitating states: they are moist, sport small, or negative values of DCIN, and give the highest precipitation rates.
3. Environmental moisture serves to modulate the precipitation by entraining more or less moisture as available, but in the current implementation of WTG, it does not seem to overcome the atmospheric stability. In other words,
 - 3.1. Unstable environments have greatly diminished moisture and precipitation; moistening the environment does not change this.
 - 3.2. More stable environments are very conducive to precipitation. Drying the environment reduces—but does not eliminate—the precipitation in the domain.
4. NGMS—which summarizes our ignorance about the relationship between convection and the convective forcing—is strongly related to the precipitation rate. In the steady state with approximately constant entropy forcing, we expect—and we observe—an inversely proportional relationship between precipitation rate and NGMS in precipitating states. The relationship between NGMS and other diagnostics, however, is not as straight-forward:
 - 4.1. There is only a slight correspondence between NGMS and atmospheric stability, which is stronger for moister environments and nearly absent for drier environments. Most likely, the biggest impact of atmospheric stability is an indirect result of modifying the vertical mass flux profile which controls lateral entrainment and detrainment of moist entropy and moisture.
 - 4.2. For the precipitating states, and for environments which are sufficiently different from RCE, there is an inverse relation between NGMS and saturation fraction. Dry states, on the other hand, all seem to exhibit small and sometimes negative values of NGMS (in agreement with *Sessions et al.* [2010]).

5.4. Multiple Equilibria

One important application of WTG experiments relates to the analogy between the smaller domain WTG simulations which exhibit multiple equilibria—either a persistent precipitating steady state or a completely dry subsiding troposphere—and the dry and moist regions of a larger domain RCE simulation with self-aggregated convection. Thus, we consider the effect of different reference environments and moisture treatments on multiple equilibria. Insight in this context may help elucidate the behavior of convection in self-aggregation simulations.

Whether or not a particular set of conditions exhibit multiple equilibria is determined by performing a set of parallel experiments in which all parameters are identical with the exception of the initial tropospheric moisture content: one experiment is initialized with the reference moisture profile, while the other is initially completely dry. If the initially moist experiment maintains persistent precipitating convection while the initially dry experiment remains dry with zero precipitation, then the set of parameters exhibits multiple equilibria. If, on the other hand, the initially dry profile develops precipitating convection—or if the initially moist profile evolves to and maintains a dry steady state—then there is a single equilibrium. We hypothesize that parameters which affect the existence of multiple equilibria in WTG experiments are also important for self-aggregation in large RCE simulations.

As demonstrated in *Sessions et al.* [2010], the model used in this experiment supports multiple equilibria in conditions similar to those used in this work. Using lateral entrainment of moisture and interactive radiation, *Sessions et al.* [2010] found multiple equilibria to exist for a significant range of wind speeds with unperturbed RCE reference profiles. In an updated version of the model, *Herman and Raymond* [2014] showed multiple equilibria occurs with static, noninteractive radiation (though not when a spectral form of WTG is implemented).

The first task is to determine whether the existence of multiple equilibria in this model depends on the parameterization of horizontal moisture advection. *Sobel et al.* [2007] demonstrated that states of multiple equilibria are sensitive to how moisture advection is parameterized; here we test this systematically with

Table 2. Table Identifying Which Moisture Treatments Exhibit Multiple Equilibria With Surface Wind Speed of 7 m s^{-1} ^a

	$\lambda_{hadv}=0$	$\lambda_{hadv}=1$
$\lambda_m=0$	NO	YES
$\lambda_m \neq 0$	NO	NO

^a“YES” means that a dry state is maintained if initiated with a dry troposphere; “NO” means that precipitation developed in spite of an initially dry troposphere. With fixed radiation, the only moisture treatment that maintains multiple equilibria is lateral entrainment.

($\lambda_{hadv}=1, \lambda_m=0$). That multiple equilibria exist for lateral entrainment in these experiments is undoubtedly a consequence of the extreme drying of the free troposphere that only occurs with this choice (Figures 10g—10i). The extreme drying is conducive to maintaining a dry state and supporting multiple equilibria. These results are summarized in Table 2.

To determine how robust multiple equilibria are with laterally entrained moisture, we repeated the experiment with zero initial tropospheric moisture, but with a surface wind speed of 10 m s^{-1} . In this case, the experiment began to precipitate and only a single equilibrium state exists. This is an important result: with static radiative cooling, multiple equilibria exists over a range of wind speeds from 5 to 10 m s^{-1} only if horizontal moisture advection is parameterized with lateral entrainment. Figure 14 shows the precipitation rate for the multiple equilibria experiments performed with laterally entrained moisture.

It is interesting to compare the results of this section with the multiple equilibria results of *Sobel et al.* [2007] and *Herman and Raymond* [2014]. *Sobel et al.* [2007] found that multiple equilibria exist for a large range of SSTs with experiments that did not explicitly parameterize horizontal moisture advection (similar to our control method); parameterizing large-scale moisture advection via a moisture relaxation reduced the range of SSTs which permitted multiple equilibria in this model. This demonstrates that different models, differences in implementing WTG, or differences in parameterizing horizontal moisture advection can produce different results with respect to multiple equilibria. *Herman and Raymond* [2014] tested multiple equilibria in the conventional WTG (as in this work) and in a version of WTG which spectrally decomposes heating (with lateral entrainment and static radiation). It is important to note that in the results of *Herman and Raymond* [2014], their model only exhibited multiple equilibria for the conventional WTG approach (as used in this work), but not in the spectrally modified implementation, and furthermore, multiple equilibria depended on the height of the boundary layer. The existence of multiple equilibria may also depend on many other model details, including domain size or the degree to which WTG is enforced [*Sessions et al.*, 2010], details of the implementation of WTG [e.g., *Daleu et al.*, 2012], or background SST [*Emanuel et al.*, 2013]. How each of these factors affects the existence of multiple equilibria is not fully understood; experiments such as this are aimed to improve the overall understanding, and especially determine which factors are representative of physical processes in the atmosphere.

Finally, to determine the sensitivity of multiple equilibria to changes in environmental stability and moisture, we performed two more experiments with lateral moisture entrainment and an initially dry troposphere: the first in a more stable environment, the second in a more moist environment. In both cases, the model produced precipitating convection and multiple equilibria were not sustained.

6. Summary

We used a cloud system-resolving model on a two-dimensional domain with the large-scale parameterized by the weak temperature gradient (WTG) approximation to investigate the response of convection to changes in the thermodynamic environment. The thermodynamic environment was initially set by vertical profiles of potential temperature and moisture in radiative convective equilibrium (RCE), and we added perturbations to change the environmental stability and moisture. For the magnitudes of perturbations explored in this work, we found that atmospheric stability dominates changes in the character of convection by prescribing the vertical motion in the domain:

1. more stable environments produce bottom heavy convection with higher precipitation rates than unperturbed profiles—even in drier environments.

different horizontal moisture advection treatments. Specifically, we run experiments initialized with zero tropospheric moisture, using unperturbed reference profiles, for each moisture treatment. All other parameters are identical to the experiments reported in previous sections (including surface wind speeds of 7 m s^{-1}). Of all the moisture treatments, the only one to maintain a dry equilibrium state over 30 days was lateral moisture entrainment

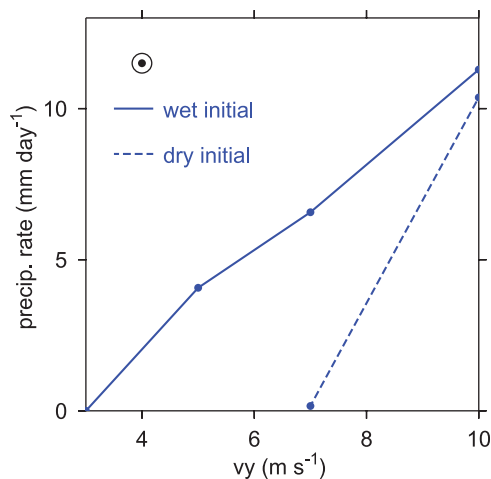


Figure 14. Precipitation rate as a function of surface wind speed for simulations which are initialized either with the reference moisture profile (solid line), or with a completely dry troposphere (dashed line). Moisture is laterally entrained in all experiments, and there is a range of wind speeds which exhibit multiple equilibria. The bulls eye in the top left indicates unperturbed reference profiles (see Figure 3).

tics: more stable environments—characterized by smaller instability indices—correlate with higher saturation fractions. These relationships hold independent of the perturbations applied to the reference environments.

Horizontal moisture advection plays an important role in the interaction between convection and the large-scale circulations. We investigate alternate parameterizations of this process, which include lateral entrainment by divergent circulations induced by enforcing WTG, a moisture relaxation which represents a parameterization of horizontal moisture advection by nondivergent circulations, a combination of both of these, and control simulations which assume horizontal advection is negligible compared to vertical advection (so lateral entrainment and moisture relaxation are both turned off). In thermodynamic environments which support precipitating convection, there is little difference in the characteristics of convection—as determined by precipitation rate, saturation fraction, DCIN, NGMS, and vertical profiles of mass flux—for different moisture treatments (except that precipitation rate is insensitive to changes in reference moisture if horizontal moisture advection is not explicitly parameterized via lateral entrainment or a relaxation to a reference profile). The most significant difference between moisture treatments is seen when the environment does not support convection (less stable environments). The most significant effects are:

1. A drastic decrease in free tropospheric moisture when horizontal moisture advection is parameterized by lateral entrainment.
2. If both lateral entrainment and moisture relaxation are turned off—so the domain is not sensitive to changes in environmental moisture—the model generates ascent in the upper troposphere which supports light precipitation. In this case, moisture and moist entropy are both imported, and NGMS is negative.

Multiple equilibria—dry or precipitating states in identical boundary conditions—are of particular interest because of the hypothesized relationship to dry and moist regions in larger domain RCE simulations where convection has self-aggregated. In this work, we investigated the sensitivity of multiple equilibria to changes in the thermodynamic environment and different parameterizations of horizontal moisture advection. Using static (noninteractive) radiative cooling, we found that the existence of multiple equilibria is sensitive to both the thermodynamic environment and choice of moisture treatment. For the parameters used in this work, our model only exhibited multiple equilibria for laterally entrained moisture in an unperturbed reference environment. Other moisture treatments exhibited only a single equilibrium, and imposing either a more stable or more moist environment destroyed the dry equilibrium state even when moisture was laterally entrained. To the extent that multiple equilibria are analogous to dry and moist regions in a self-

2. less stable environments shut off precipitation by generating descent throughout the free troposphere.

On the other hand, the environmental moisture modulates precipitation rates according to the amount of moisture available for precipitation—they can amplify or weaken vertical motion—but in general they do not change the shape of the convective profile.

Convection is characterized by a set of diagnostics that includes precipitation rate, vertical mass flux, an instability index (a measure of instability), saturation fraction, normalized gross moist stability (NGMS), and deep convective inhibition (DCIN). The shape of the vertical mass flux directly affects budgets of moisture and moist entropy in the domain, which sets the values of the diagnostic quantities. Our results show that in environments which support precipitating convection, the precipitation rate is a sensitive function of saturation fraction, and is inversely proportional to NGMS. Atmospheric stability also plays an important role in the relationship between diagnos-

aggregated RCE simulation—and to the extent that the MJO can be depicted as a manifestation of self-aggregation—these results may be significant for improving simulations of the MJO [Pritchard and Bretherton, 2014; Zhu and Hendon, 2015].

Our results are important not only for understanding the physics of tropical convection, but also for interpreting other studies which implement WTG. As far as mechanisms governing the development of deep convection, our results suggest that convection is very sensitive to the thermodynamic environment. Other large-scale forcing mechanisms, including radiative cooling, surface fluxes, or the propagation of atmospheric waves, may affect convection indirectly by modifying the thermodynamic environment. For example, easterly waves generate virtual temperature anomalies—similar to those idealized in this work—that enhance or suppress convection [Reed and Recker, 1971; Raymond and Sessions, 2007; Gjorgjievska and Raymond, 2014]. We are not suggesting that there are no direct influences on convection by these mechanisms, only that this work provides strong evidence that there is also an indirect effect which acts via a modification of the thermodynamic environment. This is significant insight given the growing use of the WTG approximation to understand different aspects of tropical convection, including tropical cyclogenesis [Raymond and Sessions, 2007] and the Madden-Julian Oscillation [Wang et al., 2013].

Acknowledgments

We thank David Raymond, Adam Sobel, Shuguang Wang, George Craig, and Saska Gjorgjievska for helpful discussions. We also thank two anonymous reviewers whose thorough critiques helped improve this manuscript. This work was supported by U. S. National Science Foundation Grants AGS-1056254, ATM-1021049, and AGS-1342001. Data used for this research are available upon request from the corresponding author; please send requests via email to sessions@kestrel.nmt.edu. The model used to generate the data is available at <http://kestrel.nmt.edu/~raymond/tools.html>.

References

- Anber, U., S. Wang, and A. Sobel (2014), Response of atmospheric convection to vertical wind shear: Cloud-system-resolving simulations with parameterized large-scale circulation. Part i: Specified radiative cooling, *J. Atmos. Sci.*, *71*, 2976–2993, doi:10.1175/JAS-D-13-0320.1.
- Blossey, P. N., C. S. Bretherton, and M. C. Wyant (2009), Subtropical low cloud response to a warmer climate in a superparameterized climate model. Part ii: Column modeling with a cloud resolving model, *J. Adv. Model. Earth Syst.*, *1*, 8, doi:10.3894/JAMES.2009.1.8.
- Bretherton, C. S., and P. K. Smolarkiewicz (1989), Gravity waves, compensating subsidence and detrainment around cumulus clouds, *J. Atmos. Sci.*, *46*, 740–759.
- Bretherton, C. S., T. Uttal, C. W. Fairall, S. E. Yuter, R. A. Weller, D. Baumgardner, K. Comstock, R. Wood, and G. B. Raga (2004), The EPIC 2001 stratocumulus study, *Bull. Am. Meteorol. Soc.*, *85*, 967–977.
- Bretherton, C. S., P. N. Blossey, and M. Khairoutdivnov (2005), An energy-balance analysis of deep convective self-aggregation above uniform SST, *J. Atmos. Sci.*, *62*, 4273–4292.
- Cohen, B. G., and G. C. Craig (2004), The response time of a convective cloud ensemble to a change in forcing, *Q. J. R. Meteorol. Soc.*, *130*, 933–944, doi:10.1256/qj.02.218.
- Daleu, C. L., S. J. Woolnough, and R. S. Plant (2012), Cloud-resolving model simulations with one- and two-way couplings via the weak temperature gradient approximation, *J. Atmos. Sci.*, *69*, 3683–3699, doi:10.1175/JAS-D-12-058.1.
- Derbyshire, S. H., I. Beau, P. Bechtold, J.-Y. Grandpeix, J.-M. Piriou, J.-L. Redelsperger, and P. M. M. Soares (2004), Sensitivity of moist convection to environmental humidity, *Q. J. R. Meteorol. Soc.*, *130*, 3055–3079, doi:10.1256/qj.03.130.
- Emanuel, K., A. A. Wing, and E. M. Vincent (2013), Radiative-convective instability, *J. Adv. Model. Earth Syst.*, *5*, 75–90, doi:10.1002/2013MS000270.
- Fuchs, Z., S. L. Sessions, and D. J. Raymond (2014), Mechanisms controlling the onset of simulated convectively coupled kelvin waves, *Tellus Ser. A*, *66*, 22107, doi:10.3402/tellusa/v66.22107.
- Gjorgjievska, S., and D. J. Raymond (2014), Interaction between dynamics and thermodynamics during tropical cyclogenesis, *Atmos. Chem. Phys.*, *14*, 3065–3082, doi:10.5194/acp-14-3065-2014.
- Herman, M. J., and D. J. Raymond (2014), WTG cloud modeling with spectral decomposition of heating, *J. Adv. Model. Earth Syst.*, *6*, 1121–1140, doi:10.1002/2014MS000359.
- Jeevanjee, N., and D. M. Romps (2013), Convective self-aggregation, cold pools, and domain size, *Geophys. Res. Lett.*, *40*, 994–998, doi:10.1002/grl.50204.
- Kuang, Z. (2008), Modeling the interaction between cumulus convection and linear gravity waves using a limited-domain cloud system-resolving model, *J. Atmos. Sci.*, *65*, 576–591.
- Kuang, Z. (2010), Linear response functions of a cumulus ensemble to temperature and moisture perturbations and implications for the dynamics of convectively coupled waves, *J. Atmos. Sci.*, *67*, 941–962, doi:10.1175/2009JAS3260.1.
- Mapes, B. E. (2004), Sensitivities of cumulus-ensemble rainfall in a cloud-resolving model with parameterized large-scale dynamics, *J. Atmos. Sci.*, *61*, 2308–2317.
- Masunaga, H. (2012), Short-term versus climatological relationship between precipitation and tropospheric humidity, *J. Clim.*, *25*, 7983–7990, doi:10.1175/JCLI-D-12-00037.1.
- Muller, C. J., and I. M. Held (2012), Detailed investigation of the self-aggregation of convection in cloud-resolving simulations, *J. Atmos. Sci.*, *69*, 2551–2565, doi:10.1175/JAS-D-11-0257.1.
- Neelin, J. D., and I. M. Held (1987), Modeling tropical convergence based on the moist static energy budget, *Mon. Weather Rev.*, *115*, 3–12.
- Peters, O., and J. D. Neelin (2006), Critical phenomena in atmospheric precipitation, *Nat. Phys.*, *2*, 393–396, doi:10.1038/nphys314.
- Pritchard, M. S., and C. S. Bretherton (2014), Causal evidence that rotational moisture advection is critical to the superparameterized Madden-Julian oscillation, *J. Atmos. Sci.*, *71*, 800–815, doi:10.1175/JAS-D-13-0119.1.
- Raymond, D. J., and Z. Fuchs (2007), Convectively coupled gravity and moisture modes in a simple atmospheric model, *Tellus Ser. A*, *59*, 627–640, doi:10.1111/j.1600-0870.2007.00268.x.
- Raymond, D. J., and Z. Fuchs (2009), Moisture modes and the Madden-Julian oscillation, *J. Clim.*, *22*, 3031–3046, doi:10.1175/2008JCLI2739.1.
- Raymond, D. J., and S. L. Sessions (2007), Evolution of convection during tropical cyclogenesis, *Geophys. Res. Lett.*, *34*, L06811, doi:10.1029/2006GL028607.
- Raymond, D. J., and D. J. Torres (1998), Fundamental moist modes of the equatorial troposphere, *J. Atmos. Sci.*, *55*, 1771–1790, doi:10.1175/1520-0469(1998)055<1771:FMMOTE>2.0.CO;2.

- Raymond, D. J., and X. Zeng (2005), Modelling tropical atmospheric convection in the context of the weak temperature gradient approximation, *Q. J. R. Meteorol. Soc.*, *131*, 1301–1320.
- Raymond, D. J., G. B. Raga, C. S. Bretherton, J. Molinari, C. López-Carrillo, and Z. Fuchs (2003), Convective forcing in the intertropical convergence zone of the eastern Pacific, *J. Atmos. Sci.*, *60*, 2064–2082.
- Raymond, D. J., S. L. Sessions, and Z. Fuchs (2007), A theory for the spinup of tropical depressions, *Q. J. R. Meteorol. Soc.*, *133*, 1743–1754.
- Raymond, D. J., S. L. Sessions, A. H. Sobel, and Z. Fuchs (2009), The mechanics of gross moist stability, *J. Adv. Model. Earth Syst.*, *1*, 9, doi:10.3894/JAMES.2009.1.9.
- Raymond, D. J., S. L. Sessions, and C. L. Carrillo (2011), Thermodynamics of tropical cyclogenesis in the northwest Pacific, *J. Geophys. Res.*, *116*, D18101, doi:10.1029/2011JD015624.
- Reed, R. J., and E. E. Recker (1971), Structure and properties of synoptic-scale wave disturbances in the equatorial western pacific, *J. Atmos. Sci.*, *28*, 1117–1133.
- Romps, D. M. (2012a), Weak pressure gradient approximation and its analytical solutions, *J. Atmos. Sci.*, *69*, 2835–2845, doi:10.1175/JAS-D-11-0336.1.
- Romps, D. M. (2012b), Numerical tests of the weak pressure gradient approximation, *J. Atmos. Sci.*, *69*, 2846–2856, doi:10.1175/JAS-D-11-0337.1.
- Sessions, S. L., S. Sugaya, D. J. Raymond, and A. H. Sobel (2010), Multiple equilibria in a cloud resolving model using the weak temperature gradient approximation, *J. Geophys. Res.*, *115*, D12110, doi:10.1029/2009JD013376.
- Sobel, A. H., and G. Bellon (2009), The effect of imposed drying on parameterized deep convection, *J. Atmos. Sci.*, *66*, 2085–2096, doi:10.1175/2008JAS2926.1.
- Sobel, A. H., and C. S. Bretherton (2000), Modeling tropical precipitation in a single column, *J. Clim.*, *13*, 4378–4392.
- Sobel, A. H., G. Bellon, and J. Bacmeister (2007), Multiple equilibria in a single-column model of the tropical atmosphere, *Geophys. Res. Lett.*, *34*, L22804, doi:10.1029/2007GL031320.
- Tulich, S. N., and B. E. Mapes (2010), Transient environmental sensitivities of explicitly simulated tropical convection, *J. Atmos. Sci.*, *67*, 923–940, doi:10.1175/2009JAS3277.1.
- Wang, S., and A. H. Sobel (2011), Response of convection to relative sea surface temperature: Cloud-resolving simulations in two and three dimensions, *J. Geophys. Res.*, *116*, D11119, doi:10.1029/2010JD015347.
- Wang, S., and A. H. Sobel (2012), Impact of imposed drying on deep convection in a cloud-resolving model, *J. Geophys. Res.*, *117*, D02112, doi:10.1029/2011JD016847.
- Wang, S., A. H. Sobel, and Z. Kuang (2013), Cloud-resolving simulation of TOGA-COARE using parameterized large scale dynamics, *J. Geophys. Res. Atmos.*, *118*, 6290–6301, doi:10.1002/jgrd.50510.
- Wing, A. A., and K. A. Emanuel (2013), Physical mechanisms controlling self-aggregation of convection in idealized numerical modeling simulations, *J. Adv. Model. Earth Syst.*, *5*, 59–74, doi:10.1002/2013MS000269.
- Zhu, H., and H. H. Hendon (2015), Role of large-scale moisture advection for simulation of the MJO with increased entrainment, *Q. J. R. Meteorol. Soc.*, doi:10.1002/qj.2510.